



Formulation, optimization and evaluation of ocular gel containing neбиволol Hcl-loaded ultradeformable spanlastics nanovesicles: In vitro and in vivo studies

Mohamed Yasser^{a,b}, Eman E. El Naggar^b, Nehal Elfar^b, Mahmoud H. Teaima^c, Mohamed A. El-Nabarawi^{c,*}, Sammar Fathy Elhabal^{d,*}

^a Department of Pharmaceutics, Faculty of Pharmacy, Port Said University, Port Said 42526, Egypt

^b Department of Pharmaceutical technology, Faculty of Pharmacy, Horus University, New Damietta 34518, Egypt

^c Department of Pharmaceutics and Industrial Pharmacy, Faculty of Pharmacy, Cairo University, Cairo 11562, Egypt

^d Department of Pharmaceutics and Industrial Pharmacy, Faculty of Pharmacy, Modern University for Technology and Information (MTI), Mokattam, Cairo 11571, Egypt

ARTICLE INFO

Keywords:

Glaucoma
Spanlastic nanovesicles (SNVs)
Nebivolol
Ketorolac
Biopharmaceutics classification system (BCSII) and Labrasol
Confocal laser scanning

ABSTRACT

The study aims to improve the ocular delivery of Nebivolol HCL (NBV) belonging to the Biopharmaceutics classification system (BCSII) by using spanlastic nanovesicles (SNVs) for ophthalmic delivery and incorporating them into hydroxypropyl methylcellulose gel with ketorolac tromethamine (KET) as an anti-inflammatory to improve glaucoma complications like Conjunctivitis. SNVs were prepared by ethanol injection technique using span (60) as a surfactant and labrasol as an edge activator (EA). The impact of formulation factors on SNVs properties was investigated using a Box-Behnken design. In vitro evaluations showed that the formulations (F1, F4, and F14), containing Span 60 and labrasol as EA (25%, 50%, and 25%), exhibited high EE% with low PS and high ZP and DI. Additionally, $61.72 \pm 0.77\%$, $58.97 \pm 1.44\%$, and $56.20 \pm 2.32\%$ of the NBV amount were released from F1, F4, and F14 after 5 h, compared to $93.94 \pm 1.21\%$ released from drug suspension. The selected formula (G1), containing F1 in combination with KET and 2% w/w HPMC, exhibited $76.36 \pm 0.90\%$ drug release after 12 h. Ex vivo Confocal laser scanning revealed a high penetration of NBV-SNVs gel that ascertained the results of the in-vitro study. In vivo studies showed a significant decrease in glaucoma compared to drug suspension, and histopathological studies showed improvement in glaucomatous eye retinal atrophy. G1 is considered a promising approach to improving ocular permeability, absorption, and anti-inflammatory activity, providing a safer alternative to current regimens.

1. Introduction

Glaucoma, the second most common cause of blindness, is characterized by increased intraocular pressure (IOP) (Abdelmonem et al., 2021; Zafar et al., 2016). In most cases, this sustained elevation in pressure is caused by the accumulation of aqueous humor in the anterior chamber of the eye due to an imbalance between its production and outflow through the trabecular meshwork. This high pressure is transferred to the posterior portion of the eye, including the retina and optic nerve head, where it leads to the gradual death of retinal ganglion cells (RGCs) and visual impairment (Esteban-Pérez et al., 2020).

The use of beta-blockers such as timolol, carvedilol, and neбиволol

(NBV) has been shown to have anti-hypertensive effects when administered systemically, according to (Olgac et al., 2021). Ophthalmic administration of NBV has also been reported to lower intraocular pressure and provide neuroprotection. However, NBV is classified as a Biopharmaceutical Classification System (BCS) class II drug, which means it has low solubility and low bioavailability due to its low water solubility and dissolution rate (Fathy Elhabal et al., 2023; Kakkar and Kaur, 2011). The elimination half-life of NBV is typically 12 h but can be prolonged in poor metabolizers.

Glaucoma patients often experience ocular symptoms including eye redness, itching, and pain as noted by (Baudouin et al., 2021). To alleviate these symptoms, ketorolac, a non-selective cyclooxygenase

* Corresponding authors.

E-mail addresses: mhamdy@horus.edu.eg, Mohamed.Yasser@pharm.psu.edu.eg (M. Yasser), mohamed.elnabarawi@pharma.cu.edu.eg (M.A. El-Nabarawi), Sammar.Fathy@pharm.mti.edu.eg, sammar_fathy2007@yahoo.com (S.F. Elhabal).

<https://doi.org/10.1016/j.ijpx.2023.100228>

Received 6 August 2023; Received in revised form 20 December 2023; Accepted 27 December 2023

Available online 16 January 2024

2590-1567/© 2023 Published by Elsevier B.V. This is an open access article under the CC BY-NC-ND license (<http://creativecommons.org/licenses/by-nc-nd/4.0/>).

inhibitor, is a safe and effective treatment for ocular inflammation and irritation (Turan-Vural et al., 2012).

Effective treatment of chronic ophthalmic disorders such as glaucoma typically requires frequent instillation of medications (Zafar et al., 2016), which may cause unfavorable side effects and decrease patient adherence, as pointed out by (Bessone et al., 2021). For this reason, there is a need for enhanced drug delivery systems that can provide sustained and long-term release in the anterior or posterior regions of the eye to improve therapy efficacy and patient adherence (Qamar et al., 2019).

The topical route of administration is preferred due to its non-invasive nature, minimal side effects, higher patient compliance, and lower cost (Koppa Raghu et al., 2020). However, various anatomical and physiological barriers in the eye hinder effective drug delivery, leading to low bioavailability of ocular drugs (Onugwu et al., 2023; Zafar et al., 2016). To overcome these challenges and improve drug delivery, there is growing interest in nanotechnology-based approaches, as highlighted by (Srivastava et al., 2023). Nanocarriers such as liposomes, niosomes, nanoemulsions, and polymeric nanoparticles have shown great potential in ophthalmic drug delivery due to their small size, biocompatibility, and ability to encapsulate both hydrophilic and hydrophobic medications (Khiev et al., 2021). These nano-delivery systems can bypass ocular drug delivery obstacles such as the corneal epithelium, conjunctiva, and blood-retinal barrier. Developing innovative nano-delivery systems for ocular drugs is a promising area of research that has the potential to revolutionize the treatment of various ophthalmic diseases (Das et al., 2022). However, it is important to note that selective limitation of ocular tissue membranes and barriers is necessary to maintain ocular homeostasis by properly functioning ocular biological barriers (Gaudana et al., 2010).

Despite this, these nanocarriers can be rejected due to their rigidity. Notably, a flexible bilayer facilitates the passage of vesicles through biological membranes and eliminates the true cause of ineffectual ocular delivery (i.e., the dense mucin layer) (Kaviarasi et al., 2023; Rathod et al., 2021). Vesicular drug delivery systems are an intriguing strategy for attaining desirable ocular delivery system characteristics such as simplicity of administration, targeted and controlled drug delivery, and exceptional permeability. The permeation rate is largely determined by the drug carrier system and the physicochemical properties of the drug molecules (Elhabal et al., 2023; Onugwu et al., 2023).

Spanlastics are a type of vesicular transporter that is biodegradable, non-immunogenic, and non-toxic. They have shown promise in enhancing drug delivery due to their flexibility, which makes them more favorable than conventional niosomal dispersions and more chemically stable than liposomes (Huang et al., 2017). By allowing for enhanced drug permeation and selective delivery of both hydrophilic and lipophilic drugs for a sustained period, Spanlastics can lead to improved therapeutic effects, patient adherence, and reduced adverse effects (Gaafar et al., 2014). There is growing interest in using Spanlastics for various drug delivery applications, including trans-tympanic delivery, ocular delivery, trans-ungual delivery, and topical distribution (Ansari et al., 2022).

Typically, Spanlastics consist of a surfactant (such as Span) and edge activators that enhance the entrapment of drugs in the vesicle and improve steric stability (Sharma et al., 2020).

Edge activators can disrupt vesicles and enhance their deformability by reducing surface tension (Duangjit et al., 2013). The high elasticity of Spanlastics enables them to increase drug permeation through various mucosal bio-membranes by compressing through membrane apertures with minimal risk of vesicular rupture (ElMeshad and Mohsen, 2016). Previous research has explored the ability of Spanlastics to enhance drug absorption in different contexts, including ocular, trans-duodenal, and transdermal (Mohammed et al., 2023a; Fahmy et al., 2019; Tayel et al., 2015). Adding permeation-enhancers such as labrasol (Capryl caproyl macrogol-8 glycerides) to Spanlastics may synergistically affect the skin and eye penetration of drugs. Labrasol, a water-soluble oil is commonly

used in topical, transdermal, and oral pharmaceutical preparations as an emulsifier and absorption promoter (Liu et al., 2009).

Gel formulations, which are composed of a liquid phase within a polymeric matrix, have become increasingly popular due to their sustained drug release, ease of application, and ability to resist various absorption conditions. Additionally, patients have the flexibility to discontinue medication as needed. By incorporating nano-Spanlastics into hydrogel, sustained drug delivery can be achieved, which improves patient compliance, prolongs the duration of drug concentration within the therapeutic range, and enables lower drug doses (Miastkowska et al., 2020; Zaki et al., 2022b).

This study aims to enhance topical administration, solubility, and bioavailability in the ocular barrier for Nebivolol HCl by developing and optimizing it in nanospanlastic vesicles (SNVs), inspired by the unique properties of Spanlastics. The selected Nebivolol HCl-loaded SNVs were evaluated, and a mixture of the selected NBV-loaded SNVs and KET was incorporated into ocular mucoadhesive gels using Hydroxypropyl methyl cellulose (HPMC K4) to prolong the duration of drug stay on the corneal surface, improve drug bioavailability, and enhance patient compliance. In vivo studies were conducted to evaluate the anti-glaucoma activity, pharmacokinetic parameters, and histopathology of corneal specimens of the selected NBV-loaded SNVs and KET gel.

2. Materials

Nebivolol HCl was supplied by Virdev Intermediates Pvt. (India). Ketorolac tromethamine was a kind gift from Amriya for Pharmaceutical Industries, Alexandria, Egypt. Labrasol (HLB = 8–12) was obtained as a gift by gatefosee (Saint-Priest, France). Sorbitan monostearate (Span 60) (HLB = 4.7) was purchased from Oxford Lab Chemicals (Mumbai, India). Absolute ethyl alcohol and Polyoxyethylene (20) Sorbian monooleate (Tween 80), Hydroxy propyl methyl cellulose K4 (HPMC) was purchased from Acros Organics (New Jersey, USA). Pluronic® F127 was purchased from Sigma-Aldrich (St. Louis, MO). Sodium lauryl sulfate (SLS) was purchased from El-Nasr Chemical Co. Company (Cairo, Egypt). Spectra Pore® dialysis membranes (Molecular weight cut-off 12,000–14,000 Da) were purchased from Spectrum Laboratories Inc. (Rancho Dominguez, CA, USA). NaCl, NaHCO₃, and CaCl₂·2H₂O were purchased from El-Nasr Pharmaceutical Chemicals Co., Egypt. All the remaining chemicals were of analytical grade.

3. Method

3.1. Preparation of NBV-loaded SNVs

For the preparation of NBV-loaded SNVs, ethanol injection method was implemented as it is a simple and reproducible process (Badria et al., 2020; Jaafar-Maalej et al., 2010). As shown in Table 3, the design comprised of 17 experimental runs, Quadratic response surface model (generated by the Box–Behnken design) using Design Expert software, Version 11.0 (Stat-Ease, Inc., Minneapolis, Minnesota, USA). Span 60 was used as the nonionic surfactant with labrasol as an EA at different concentrations (total weight 200 mg). To acquire a transparent solution, NBV (10 mg) and span 60 were carefully dissolved in a specific amount of absolute ethanol and sonicated for 5 min at 80 °C in an ultrasonic water bath (water-bath ultrasonic, El masonic E 30H, Elma, Schmidbauer GmbH, Singen, Germany). The ethanolic solution was injected cautiously using a syringe pump at a flow rate of 1 mL/min (Jiang et al., 2020) into the aqueous medium containing labrasol at 75 °C while being continuously stirred on a magnetic stirrer (Jenway 1000, Jenway, UK) until the formation of a milky Spanlastics dispersion (20 mL). To improve the evaporation of any residual alcohol, the Spanlastics dispersion was stirred for an additional four hours. The dispersions of NBV-loaded SNVs were then sonicated at an amplitude of 70% to reduce the particle size. The SNVs were then stored overnight at 4 °C for use in subsequent investigations.

3.2. Characterization of NBV-loaded SNVs

3.2.1. Assessing the deformability index (DI) of the vesicles

The elasticity of SNVs was studied by extrusion at a pressure of 2.5 bars and a pore size of 100 nm within a nylon membrane filter for three minutes. Using Zetasizer (ZEN 3600, Malvern Instruments Limited, UK), the vesicle size of various formulae, before and after filtration was determined. Using the following equation (Shoman et al., 2023):

$$DI = J(r_v / r_p)^2$$

where J is the amount of the extruded formulation, r_v : the vesicle size of the formulation (after extrusion) and r_p : the pore size of the nylon membrane filter.

3.2.2. Entrapment efficiency (EE%)

Using the indirect technique, the EE% of NBV-loaded SNVs was calculated. 1 mL of NBV-loaded SNVs was centrifuged for 2 h at 10,000 rpm at 4 °C (Cooling centrifuge, Sigma, GmbH, Germany). The concentration of free NBV was determined by UV spectrophotometer (JENWAY, Bibby Scientific Ltd., Stone, Staffs, ST15, 0SA, U-K) at a predetermined λ_{max} 282 nm after passing the supernatant via a 0.22 μ m pore size nylon membrane filter (Nylon Acrodisc, Gelman Sciences Inc., Ann Arbor, MI, USA).

EE% was calculated as follows (Abdelmonem et al., 2021; Al-Shoubki et al., 2023a):

$$EE = (\text{Total amount of NBV} - \text{Amount of free NBV}) \times 100 / \text{Total amount of NBV}$$

3.2.3. Particle size (Ansari et al.), zeta potential (ZP) of NBV-loaded SNVs

PS measurements were used to investigate the colloidal properties of nanoplastics dispersions loaded with NBV. To achieve the desired scattering intensity, 0.1 mL of NBV-loaded SNVs were diluted with deionized water (10 mL). Using a zeta sizer (ZEN 3600, Malvern Instruments Limited, UK) particle size analyzer, the size and ZP of NBV-loaded SNVs were then measured (Elhabal et al., 2023; Sammar Fathy Elhabal et al., 2023b). Various measurements were taken in triplicate, and the mean of three runs was calculated.

3.3. Statistical analysis

A Box–Behnken design was conducted using Design Expert software, Version 11.0 (Stat-Ease, Inc., Minneapolis, Minnesota, USA) to optimize the seventeen NBV-loaded SNVs and investigate the relationship between the selected independent variables and various responses. As shown in Table 1, independent variables X1, X2, and X3 (the sonication time, labrasol and ethanol percentage), respectively were considered.

Table 1

The independent variables levels used to formulate NBV-loaded SNVs.

Factors (independent variables)	Levels		
	(Low)	(Medium)	(High)
	−1	0	1
X1: sonication time (Min)	1	5.5	10
X2: Edge Activator (EA%)	0	25	50
X3: Organic solvent %	20	50	80
Response (Dependent Variable)	Desirability Constraints		
Y1: Entrapment efficiency (%EE)	Maximize		
Y2: Size of vesicles	Minimize		
Y3: Zeta potential (ZP)	Maximize		
Y4: Deformability index (DI)	Maximize		

The dependent variables were the percentage of entrapment efficiency (EE%, Y1), particle size (PS, Y2), zeta potential (ZP, Y3), and deformability index (DI, Y4). Each factor was assessed at three levels (−1, 0, and 1) that corresponded to the lower, medium, and upper levels, respectively (Elhabal et al., 2023; Al-Shoubki et al., 2023b).

3.4. Identifying the optimum formula

Applying Design-Expert® software, numerical optimization was utilized to detect acceptable factors besides disregarding insignificant ones ignoring insignificant ones. The highest EE% and ZP (absolute value) were chosen, along with the lowest PS and highest DI. According to the obtained results, the optimum formulae were chosen and then subjected for further investigation (Sammar Fathy Elhabal et al., 2023b).

3.5. Morphological characteristics of the optimized formulae

3.5.1. Transmission electron microscopy (TEM)

Using TEM at an accelerating voltage of 160 kV, the morphological properties of the optimized SNVs were investigated after extrusion. SNVs dispersion in deionized water was appropriately diluted and sonicated for uniform distribution. The dispersion was then put on a carbon-coated copper grid and air-dried (Das et al., 2017). Then, pictures of SNVs were captured using TEM and analyzed utilizing imaging viewer software.

3.6. Solid characterization of the optimized NBV-loaded SNVs

Solid Characterization of the Optimized Formulae was examined employing Fourier transform-infrared spectroscopy (FT-IR) and differential scanning calorimetry (DSC). The optimized formulae were freeze-dried (Freeze dryer, SIM FD8-8 T, SIM International, USA). Then, it was examined in comparison to samples of NBV, Span, labrasol and their physical mixture (PM).

3.6.1. Fourier transform-infrared spectroscopy (FT-IR)

FT-IR was carried out with FT-IR Spectrophotometer (Thermo Fisher Scientific iS10 Nicolet). Samples (3 mg) of NBV, span 60, Labrasol, drug-polymers PM, plain SNVs, and the selected SNVs were blended with potassium bromide and compacted into pellets with KBr in a hydraulic press (Kimaya Engineers, Maharastra, India) to identify any interactions between the formula's components and the drug. The range of scanning was 4000 to 400 cm^{-1} (Ali et al., 2014; Elhabal et al., 2023).

3.6.2. Differential scanning calorimetry (DSC)

The physicochemical condition of NBV and the potential for drug-excipient interactions were characterized by DSC analysis using a Shimadzu DSC 60 (Japan, Kyoto). Aluminum pans containing 3 mg samples of NBV, span 60, Labrasol, drug-polymers PM, plain SNVs, and the selected SNVs formulation were sealed. Samples were heated at a scan rate of 10 °C/min from 30 to 450 °C to create the corresponding thermograms (Mazyed and Zakaria, 2019).

3.7. In vitro release study of the optimum NBV-loaded SNVs

Using membrane diffusion, the in vitro release behavior of NBV-loaded SNVs was investigated (Farghaly et al., 2017). The semi-permeable cellulose membrane was pre-hydrated using simulated tear fluid (STF; made with sodium chloride-0.67 g, sodium bicarbonate-0.20

g, calcium chloride dihydrate –0.008 g in distilled water q.s 100 mL) for 24 h at room temperature. Rubber bands connected the glass cylinder at the dissolving device's tip (USP apparatus II, Copley NG4 2JJ, Nottingham, UK) to the cellulose membrane. To guarantee sink conditions, 500 mL of STF and 1% Sodium lauryl sulphate (SLS) were used as the receptor medium. The medium for the receptor was agitated at 75 rpm and maintained at 37 ± 0.5 °C. NBV (10 mg) or an equivalent amount of the lyophilized and redispersed optimized formula was introduced in the donor chamber over the cellulose membrane. In an effort to maintain sink condition, after taking 3 mL aliquots at predetermined intervals (0, 0.5, 1, 2, 3, 4, 5, 6, 7, 8, 9, 10, 11, and 12 h), it was replaced with an equivalent volume of new release medium. (Mazyed and Zakaria, 2019). The withdrawn samples were filtered through a 0.22 μ m nylon membrane filter, diluted, and then examined using a UV spectrophotometer at a predetermined λ_{max} 282 nm. The experiments were done in triplicate. The results are presented as mean values \pm SD.

3.8. Release kinetics

Several mathematical models, such as the zero-order, first-order model, the Higuchi diffusion, and the Korsmeyer-Pappas equation were applied to determine the most suitable kinetic model and the mechanism of NBV in vitro release from the optimized SNVs. The greatest value of the correlation coefficient (R^2) indicated the sequence of drug release (Van Haute et al., 2019).

3.9. Stability study

The optimized SNVs formulae were stored at 25 ± 1 °C and 4 ± 1 °C, respectively for three months. Samples were then obtained, and the mean PS, ZP (measured using a Zeta-sizer ZEN 3600, Malvern Instruments Limited, UK), and EE%, were examined. The experiments were performed in triplicate, GraphPad Prism software (GraphPad Instate Software, Inc. USA), was used for employing the ANOVA test and the Tukey-Kramer multiple comparisons test, at a significance level of $P < 0.05$ (Elhabal et al., 2023).

3.10. Compatibility study

To investigate the intermolecular interactions between KET and NBV, FT-IR was conducted with FT-IR Spectrophotometer (Thermo Fisher Scientific iS10 Nicolet) as mentioned above (Abdeltawab et al., 2021).

3.11. Formulation of NBV-loaded SNVs and KET gel

Six gel formulae were prepared to contain the selected NBV-loaded SNVs (F1, F4, and F14) and ketorolac tromethamine as an anti-inflammatory (Table 2). To prepare gel formulations, HPMC K4 at a concentration (2% and 4% W/W) was used as a mucoadhesive polymer that has the benefit of prolonging the residence time at the application site for sustained drug delivery with 12% pluronic F127 (Pandey et al., 2021). HPMC and pluronic F127 were dissolved gradually in deionized water containing a combination of NBV-loaded SNVs equivalent to (10 mg NBV) and 0.5% w/w KET using a magnetic stirrer at medium speed.

Table 2
Composition of NBV-loaded SNVs and KET formulated into gel.

Formula*	NBV-loaded SNVs.5%	HPMC K4 (%W/W)
G1	F1	2
G2	F1	4
G3	F4	2
G4	F4	4
G5	F14	2
G6	F14	4

* Each formula contains 0.5% w/w KET.

The mixture was stirred till the development of a gel base, then permitted to equilibrate overnight. Centrifugation has eliminated any confined air bubbles in the gels (Qi et al., 2022).

3.12. Evaluation of the prepared NBV-loaded SNVs and KET gel

3.12.1. Visual inspection

The developed formulae were inspected visually on a black-and-white background for physical properties such as color, clarity, and homogeneity (Zafar et al., 2022).

3.12.2. pH measurement of the prepared gels

The pH of each formula was measured three times using a pH meter (3505–Jenway, Bibby Scientific Ltd., Dunmow, UK) and the average of the three values was calculated (Teaima et al., 2021; Zafar et al., 2022).

3.12.3. Determination of drug content

Using an incubator shaker, 1g of the prepared gel was mixed with 100 mL of a suitable solvent (methanol). After filtering the solution, withdrawing and diluting aliquots, the absorbance was measured. The drug content of NBV was estimated using the calibration curve-derived procedure constant at λ_{max} 271 nm for NBV in combination with KET by first derivative spectroscopy (Sammar Fathy Elhabal et al., 2023b; Hallan et al., 2020; Salem et al., 2020).

3.12.4. Gelation time and the sol-gel transition temperature (Tsol-gel)

Using the test tube inversion approach, the formulations' T_{sol-gel} was ascertained. In an electric water bath, formulations (2 mL) were heated by increments of 2 °C or 0.5 °C in the T_{sol-gel} zone. The formulations were checked for gelation, which was defined as the point at which tilting the test tube 90° caused the liquid meniscus to stop moving. Gelation time is the amount of time needed for all of the liquid to fully transform into gel form, at which point gelation is noticed (Khan et al., 2015).

3.12.5. Evaluation of rheological properties of the prepared gels

The prepared NBV-loaded SNVs and KET Gel were using a rotating cone-and-plate Brookfield viscometer. On the plate, about 0.5 g of the tested formula was added and left until the cone temperature reached 25 ± 1 °C. The measurements were carried out at speeds ranging from 1 to 35 rpm, with 10 s between each speed setting, and then in decreasing order. The obtained formulas' rheograms were plotted, with the y-axis representing shear stress and the x-axis representing shear rate. For each of the investigated formulas, the individual rheological data [min, max, Farrow's constant (N), and hysteresis loop area (H.A)] were determined. To estimate the rheological behavior of each formula, the rheological data were evaluated using Farrow's equation (Teaima et al., 2021) and Power law equation (Ismail et al., 2020):

Farrow's equation:

$$\text{Log } D = N \log S - \text{Log } \eta$$

where: **D**: Shear rate (sec^{-1}), Shear Stress (dyne/cm^2), **N**: Farrow's constant, and **η** : Viscosity (cp).

N (Farrow's constant) is the slope of log D against log S plot, which indicates the deviation from Newtonian flow. When N is less than one, it indicates dilatant flow (shear rate thickening). If N is greater than one, it indicates pseudoplastic flow (shear rate thinning).

Power law equation:

$$\bar{U} = \eta \gamma^n$$

where: **γ** : Shear rate (sec^{-1}), **\bar{U}** : Shear Stress (dyne/cm^2), **n**: Power constant, and **η** : a constant called the consistency index (apparent viscosity).

In case of Newtonian behavior, $n=1$. Whereas in case of (shear-thinning), $0 < n < 1$. In case of dilatant flow (shear-thickening), $n > 1$.

3.12.6. *In vitro* release of the developed NBV-loaded SNVs with KET gels

NBV release from NBV-loaded SNVs and KET combination gel in comparison with NBV gel as control was conducted in the same manner discussed above. Drug-released percentages were determined spectrophotometrically at a predetermined λ_{max} 282 nm for NBV, and 271 nm for NBV in combination with KET by first derivative spectroscopy.

3.13. *Ex-vivo* confocal laser scanning microscopy (CLSM)

After topical administration, the substance under examination's ocular biodistribution was qualitatively assessed using CLSM (LSM 710, ZEN 2.3, Carl Zeiss, Germany). Fluorescent RhB was present in the SNVs rather than water. RhB was dissolved in SNVs and a polymeric solution. In the study on ocular absorption, male Wistar albino rabbits were used. Each of the four sets I got RhB solution, II received RhB-loaded drug solution, III received RhB-loaded SNVs, and VI received RhB-loaded SNVs gel had three rabbits assigned to them. An hour after treatment, the rabbits were slaughtered, and their separated eyes were cleaned with ringer's solution. On slides, sliced ocular tissues were analyzed using CLSM. At 543 nm, the argon excitation laser was used. The ZEN software took and examined pictures (Ali et al., 2014).

3.14. *In vivo* evaluation of the combination NBV and KET in the developed NBV-loaded SNVs with KET gels

3.14.1. Animals

In this experiment, a healthy adult male (2–2.5 kg) New Zealand albino rabbits with normal eyes were used. The rabbits had unrestricted access to food and water and were housed in a temperature-controlled room (22–25 °C) with a 12 h/12 h light/dark cycle. Experiments were conducted by the guidelines of the Research Ethics Committee and were approved by the Ethics Committee (PI 2688 on 27/4/2020).

3.14.2. Eye irritancy test (Draize test)

Six rabbits were used for this test with three rabbits in each group to determine how irritating the optimized formula was to them (Draize, 1944; Shivakumar et al., 2007). The first group received F1 (The optimum SNVs formula) while the second received G1 (the optimum gel formula) respectively. Two drops (100 μ L) equivalent to 10 mg of NBV and KET of the tested formula were installed in the left eye particularly in the conjunctival sac, as well as the right eye was reserved as control by applying saline at intervals 0, 1, 2, 3, 4, 5, 6, 24, 48, and finally at 72h then 7, 14, and 21 days after installation, each eye of rabbit was examined to assess the irritation grade. Following delivery when a score of zero was recorded at a predetermined interval, the evaluation of the ocular irritation score was carried out. Draize test applies a scoring system varying from 0 (no irritation) to 3 (maximum redness and irritation) (Shokry et al., 2018; Tayel et al., 2013).

3.14.3. Pharmacokinetic study

Rabbits were randomly divided into four groups: group one received NBV suspension, group two received a solution of the optimum NBV-loaded SNVs (F1), group three received a combination of KET and the optimum NBV-loaded SNVs (F1), and group four received an optimum combination of KET and NBV-loaded SNVs gel (G1). The rabbits were kept anesthetized with an injection of sodium pentobarbital (30 mg/kg) into the marginal ear vein. After each formula was injected at a concentration of 100 μ L, then 100 μ L of aqueous humor was collected after 15, 30, 60, 120, 240, and 360 min using a 1 mL insulin needle and kept in a centrifuge tube. The protein was precipitated by combining 0.5 mL of methanol with a vortex mixer. After centrifuging the precipitate for 10 min at 10,000 rpm, the protein was separated and the drug concentration was measured in the supernatant by LC-MS (Mob phase: 80% Acetonitril+20% 0.01% formic acid in water, Column: Waters Sunfire C18 50 mm 5 μ m, Extraction: 0.5 mL plasma +100 μ L (200 ng/mL). Torosemide as internal std. + 4 mL Ethyl acetate, vortex and centrifuge,

decant the organic layer and dry under vacuum then reconstitute in 200 μ L mobile phase and inject in the LC-MS/MS + ve mode using Torosemide as Internal std). The pharmacokinetic parameters were determined by a noncompartmental procedure using WinNonlin pharmacokinetic software (Software version, Certara Inc., Princeton, NJ, USA).

3.14.4. Pharmacodynamic study (intraocular pressure measurement)

The rabbits with paclitaxel eye drops® were topically anesthetized. Each eye was injected with a solution of dexamethasone (0.025%) in saline. If the *Intraocular Pressure* (IOP) was more than the typical upper limit of 24.4 mmHg and persisted for a week, the model was considered successful (Khallaf et al., 2022). Rabbits were randomly divided into four groups (six rabbits per group): group one was treated by NBV suspension, group two was treated with the optimum NBV-loaded SNVs (F1), group three was treated by a combination of KET and the optimum NBV-loaded SNVs (F1), and group four treated with optimum combination of KET and NBV-loaded SNVs gel (G1). Paclitaxel ocular drops were used to locally anesthetize the rabbits. Each rabbit's right eye was treated separately with each formula and the left eye was used as a fake control group. The intraocular pressure was measured for 4 days, and the results of reducing the IOP were compared. The process was performed twice with each time being separated by a week of washing. The equation shown below can be used to obtain a % reduction in IOP (Ali et al., 2014; Ammar et al., 2009):

$$\% \text{Decrease in IOP} = \frac{\text{IOP control eye} - \text{IOP dosed eye}}{\text{IOP Control eye}} \times 100$$

SPSS 17 software ®was used to calculate the full percentage decrease in IOP and mean residence time.

3.14.5. Histopathological examination

Following the pharmacokinetic and pharmacodynamic studies, phenobarbital sodium was injected into a marginal vein to cause the rabbits' death. Following the removal of the eyes, 10% formalin was applied. Tissue samples were prepared by being cut, cleaned, and then dehydrated in xylene. After being dehydrated, the samples were clarified, encapsulated in paraffin blocks, and at a thickness of 4–6 m they were sectioned. Hematoxylin and eosin (H&E) staining and deparaffinization with xylol allowed for histological evaluation of the collected tissue samples via an electric light microscope (Bancroft, 2013).

3.15. Data statistica analysis

The one-way analysis of variance (ANOVA) test was carried out to assess the significant difference between the formulas' outcomes. The level of significance was set at 0.05 and ($p < 0.05$).

4. Results and discussion

4.1. Analysis of the Box–Behnken experimental design of NBV-loaded SNVs

The components and responses (Y1 (EE%), Y2 (PS), Y3 (ZP), and Y4 (DI) of NBV-Loaded SNVs were developed using a *Box–Behnken* design are shown in Table 3 and Fig. 1. By comparing the factor coefficients, regression equations revealed the effect of multiple independent factors on the investigated responses. The positive sign preceding the factor coefficients indicated a positive impact on the examined responses, while the negative sign indicated a negative impact (Shoman et al., 2023).

Table 4 reveals that the adequate precision values for Y1, Y2, Y3, and Y4 in the current model are >4 (18.02, 33.86, 10.80, and 21.03, respectively). Therefore, the selected model could be utilized effectively to navigate the design space (Al-Shoubki et al., 2023a, 2023b). The predicted R^2 was measured to ascertain the predictability of the

Table 3
Measured responses of NBV-loaded SNVs.*

Formula	Variables								
	Independent			Dependent					
	Sonication time (X1)	Labrasol % (X2)	Ethanol % (X3)	EE% (Y1)	PS (Y2)	ZP (Y3)	DI (Y4)		
F1	0	0	0	60.17 ± 0.09	415.97 ± 28.26	-40.33 ± 0.36	36.11 ± 1.67		
F2	-1	0	-1	65.72 ± 0.15	626.90 ± 45.90	-34.00 ± 1.85	36.85 ± 1.90		
F3	0	0	0	58.07 ± 0.31	415.97 ± 28.26	-37.03 ± 0.60	36.86 ± 3.83		
F4	1	1	0	49.67 ± 0.55	310.23 ± 12.01	-32.80 ± 0.29	42.74 ± 5.56		
F5	-1	1	0	44.45 ± 1.05	566.30 ± 0.10	-34.00 ± 0.16	37.92 ± 2.24		
F6	0	-1	1	77.72 ± 0.15	1083.67 ± 113.46	-68.40 ± 0.98	19.30 ± 1.75		
F7	1	-1	0	45.63 ± 0.76	247.73 ± 12.00	-60.10 ± 0.92	14.22 ± 0.30		
F8	0	0	0	56.04 ± 0.52	403.60 ± 39.92	-38.90 ± 3.87	38.06 ± 0.64		
F9	0	1	1	50.85 ± 0.98	699.13 ± 100.36	-22.33 ± 0.77	52.30 ± 0.00		
F10	0	1	-1	53.44 ± 6.16	745.17 ± 28.28	-27.70 ± 2.35	39.37 ± 4.26		
F11	0	0	0	55.37 ± 0.05	415.97 ± 28.26	-28.13 ± 1.69	43.02 ± 11.68		
F12	-1	-1	0	74.89 ± 0.96	870.30 ± 5.30	-65.63 ± 0.00	19.84 ± 17.13		
F13	0	0	0	60.70 ± 0.69	478.57 ± 62.25	-45.87 ± 1.10	40.11 ± 5.09		
F14	1	0	-1	55.84 ± 0.85	237.83 ± 9.95	-29.20 ± 0.24	35.89 ± 3.77		
F15	0	-1	-1	56.89 ± 3.22	691.20 ± 80.71	-66.13 ± 2.25	20.20 ± 0.94		
F16	1	0	1	57.37 ± 0.23	345.37 ± 23.82	-32.83 ± 0.57	46.37 ± 0.00		
F17	-1	0	1	72.42 ± 2.13	954.20 ± 118.70	-43.73 ± 1.10	41.76 ± 4.52		
Independent Variables				Low (-1)				Medium (0)	High (1)
X1: Sonication time (min)				1				5.5	10
X2: Edge activator (%)				0				25	50
X3: Organic solvent (%)				20				50	80

Note: The values are expressed as mean ± SD. Abbreviations: EE: entrapment efficiency, PS: particle size, ZP: zeta potential and DI: Deformability index.

* All formulations contain 10 mg NBV.

response value. Adjusted R^2 is an altered form of R^2 that indicates how well the selected model fits the observed data. To be in reasonable agreement, the adjusted and predicted R^2 statistics should have values within 0.20 of one another (Al-Shoubki et al., 2023a).

The R^2 , predicted R^2 , and adjusted R^2 values for different responses are quite high, as shown in Table 4. Moreover, it is obvious that the predicted R^2 values of different responses closely resembled the adjusted R^2 values. These results indicate that the data gathered is statistically reliable and an outstanding match with the obtained data.

4.1.1. The effect of formulation variables on EE%

The EE% is an essential measurement for evaluating both the drug retention and stability of nanovesicles (Fang et al., 2001). As shown in Table 3, EE% of NBV-loaded SNVs ranges from 44.45% ± 1.05 to 77.72% ± 0.15. The effect of sonication time (X1) on the EE% of NBV in the prepared SNVs was significantly negative ($p < 0.001$). The EE% of prepared SNVs decreased markedly after increasing the sonication from 1 min to 5.5 and 10 min. This may be the result of a decrease in nanovesicle particle size. During the disruption and re-aggregation of SNVs, the drug can migrate to the external aqueous environment containing surfactant and remain in the aqueous phase via micellar solubilization, as opposed to being entrapped in the SNVs (Zaki et al., 2022a). Badria et al (Badria et al., 2020) reported similar findings in their study about the formulation of nanospanlastics for topical delivery of a natural leukotriene Inhibitor (3-Acetyl-11-Keto-β-Boswellic Acid). They discovered that increasing the sonication time decreased the nanovesicle size and concurrently decreased the EE%.

There is a statistically significant ($p < 0.0001$) correlation between the percentage of EA (X2) and the percentage of drug entrapment within the SNVs. Increasing the Labrasol percentage resulted in decreasing the size of the SNVs, thereby reducing the space available for NBV entrapment. Additionally, Labrasol increased the drug's getting out to the surrounding aqueous medium, resulting in a decrease in EE% (Bakhaidar et al., 2022). There was a positive impact of the organic solvent (X3) concentration on drug EE% ($p < 0.05$). This means that when the organic solvent concentration increased, the particle size and the EE% increased. In other words, it was reported that decreasing hydration volume decreases drug leakage and consequently decreases EE% (Abdelbary and AbouGhaly, 2015).

The regression equation was:

$$EE(Y1) = +58.07 - 6.12 \times 1 - 7.09 \times 2 + 3.31 \times 3$$

4.1.2. The effect of formulation variables on PS

Table 3 illustrated that the PS of NBV-loaded SNVs ranged between 237.83 ± 9.95 nm and 1083.67 ± 113.46 nm. PS of the NBV-loaded SNVs prepared was significantly affected by sonication time (X1), EA concentration (X2), and organic solvent concentration (X3). The PS of the formulated NBV-loaded nanovesicles decreased significantly ($p < 0.0001$) as the sonication time (X1) increased. Consistent with previous research Elsherif et al. (Elsherif et al., 2017) who found that the sonication time had a negative effect on the vesicle size of Terbinafine Hydrochloride-loaded SNVs.

The statistical analysis revealed that EA% (X2) had a significant impact on the PS of the prepared formulae ($p < 0.05$). It was evident that as the EA content of the prepared vesicles increased, their PS decreased. Similar to the results obtained by Shamma et al., the use of high EA concentrations will reduce the interfacial tension, resulting in the formation of smaller particles (Shamma et al., 2019). In addition, the small PS obtained at high EA levels may be due to the formation of mixed micelles, which have a smaller diameter than vesicles (Mohammed et al., 2023a; Elhabal et al., 2022; van den Bergh et al., 2001).

Regarding the PS of formulated NBV-loaded SNVs, it was found that it increased significantly ($p < 0.0001$) with increasing organic solvent concentration (X3). In agreement with Song et al., (Song et al., 2006) this occurs because a fully water-soluble solvent (Ethanol) leads to formation of nanoparticles with large particle sizes.

The regression equation was:

$$PS(Y2) = +426.01 - 234.57 \times 1 - 71.51 \times 2 + 97.66 \times 3$$

4.1.3. The effect of formulation variables on ZP

Zeta potential measures the attraction or repulsion of vehicles. Consequently, it can be utilized to forecast the nanovesicle's stability. Extremely stable systems have zeta potential values greater than +30 or less than -30 (Zaki et al., 2022a). Results demonstrated the effect of various independent variables (X1, X2, and X3) on the ZP of the NBV-loaded SNVs. Zeta potential values for all SNVs ranged from -68.40 ±

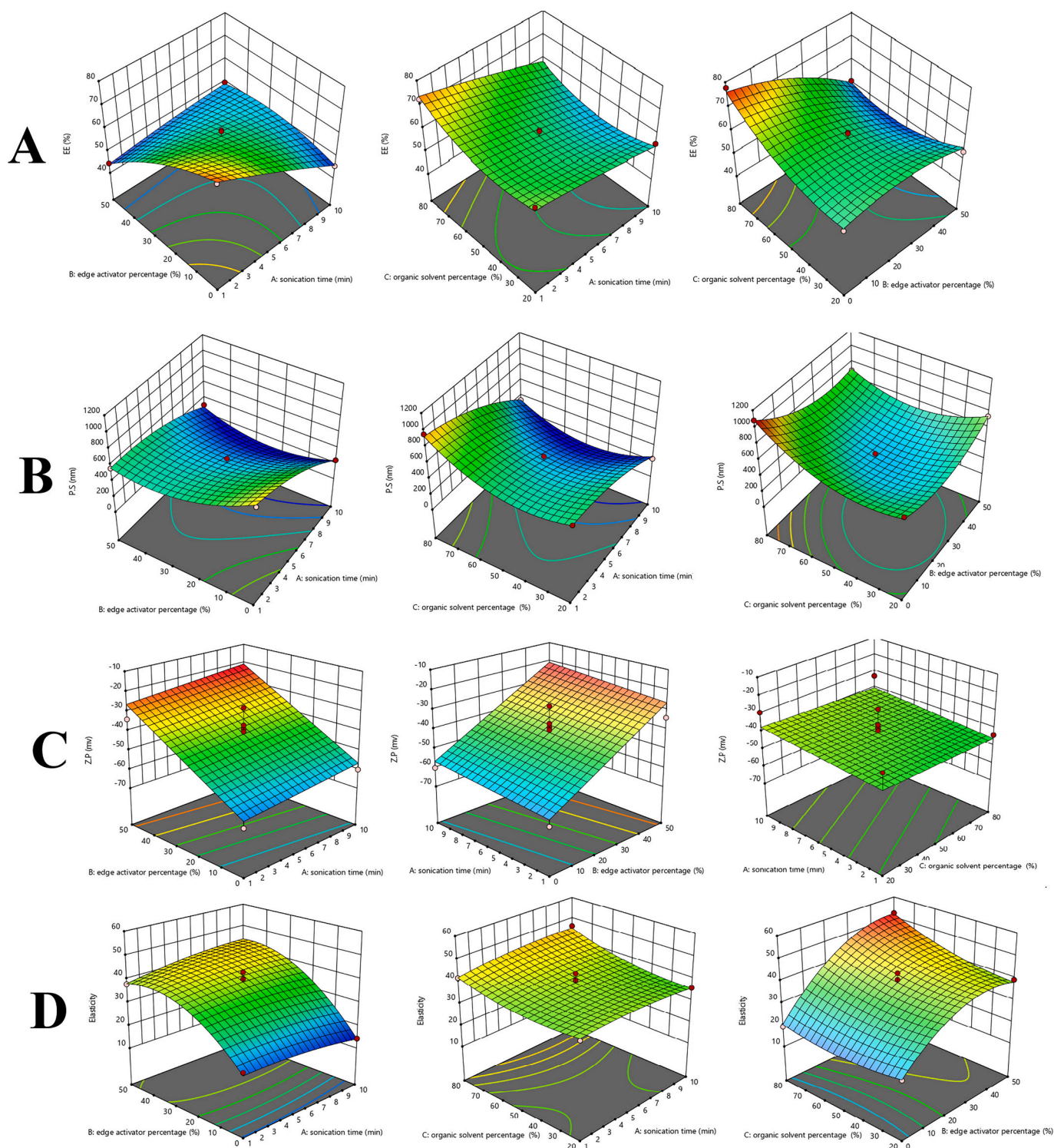


Fig. 1. Impacts of independent variables on the a) EE%, b) PS, c) ZP, d) DI of prepared NBV-loaded SNVs: 3D.

0.98 mV to -22.33 ± 0.77 mV (Table 3). According to the regression equation, ZP values are substantially influenced only by the percentage of EA (X2) ($p < 0.0001$) while X1 (sonication time) and X3 (ethanol %) were insignificant. The addition of labrasol is always responsible for the negative charge due to the presence of fatty acids (Manca et al., 2014).

The regression equation was:

$$ZP (Y3) = -41.60 + 2.80 \times 1 + 17.93 \times 2 - 1.28 \times 3$$

4.1.4. The effect of formulation variables on DI

Regarding crossing biological membranes, elastic vesicles are distinguished from other conventional colloidal carriers by their ability to deform (Elhabal et al., 2022). It is well-known that the elasticity of vesicles can be accomplished by including suitable EAs in the vesicle bilayer. Elastic vesicles, when subjected to a water gradient, can squeeze through pores much smaller than their diameters (Mohammed et al., 2023). The produced SNVs had DI values between 14.22 ± 0.30 to 52.30 ± 0.00 g as shown in Table 3. The results showed that the DI of the

Table 4

The results of Box–Behnken experimental design of NBV-loaded SNVs.

Responses	R ²	Adjusted R ²	Predicted R ²	Adequate precision
Y1: EE %	0.9742	0.9410	0.8143	18.02
Y2: PS nm	0.9927	0.9834	0.9348	33.86
Y3: ZP mv	0.7648	0.7106	0.5716	10.80
Y4: DI	0.9784	0.9507	0.9042	21.03

Abbreviations: R², R-squared or the coefficient of determination; EE, entrapment efficiency of NBV within the SNVs; PS, the particle size of NBV-loaded SNVs; ZP, Zeta potential of NBV-loaded SNVs; DI, Deformability index of NBV-loaded SNVs.

produced vesicles was not significantly affected by the sonication time (X1), however, the percent of EA (X2) has a significant effect on DI ($p < 0.0001$). This could be because of the high concentration of EA, which causes fluidization of the vesicle bilayer resulting in increasing the DI of SNVs. This may be also explained by considering the nature of the EA embedded in the vesicle membrane; membranes with less bulky EA tend to be elastic (El Zaafarany et al., 2010; Elhabal et al., 2022). In addition, the concentration of the organic solvent has a significant effect on the DI ($p < 0.05$). On increasing the organic solvent concentration (X3), the DI increases.

The regression equation was:

$$DI (Y4) = +38.84 + 0.36 \times 1 + 12.34 \times 2 + 3.43 \times 3$$

4.1.5. Optimization of NBV-loaded SNVs

The optimization process is applied to establish systematic approaches for obtaining the ideal combinations required to prepare an outstanding pharmaceutical formulation. It entails analyzing the effect of various independent variables on the properties of pharmaceutical preparations, followed by the selection of the optimal formula. (Mazyed et al., 2021). Selecting the best formulae for NBV-loaded SNVs could be achieved by optimizing multiple factors in relation to a set of desirability criteria (Basalious et al., 2010). The prepared NBV-loaded SNVs formulations were optimized for the EE% (Y1), PS (Y2), ZP (Y3), and DI (Y4). Maximizing EE%, ZP, and DI while minimizing PS was the goal of the optimization process. F1, F4, and F14 had been selected as the optimum formulae.

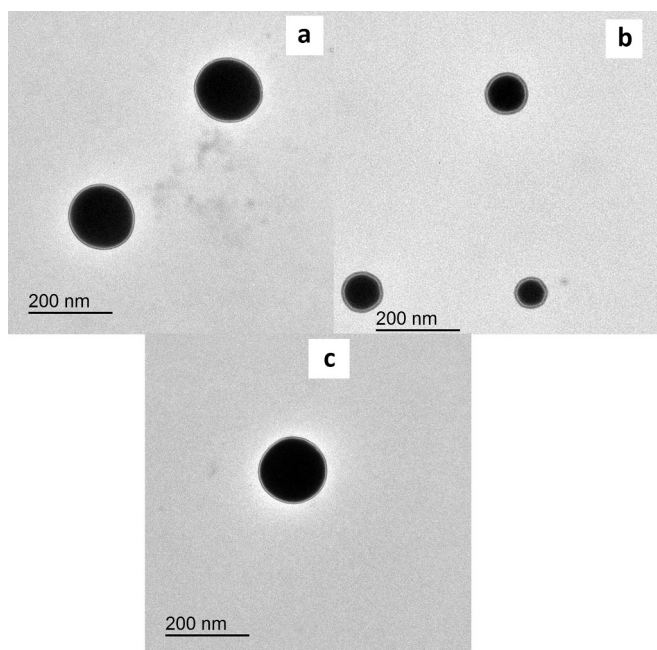


Fig. 2. TEM microphotographs of the optimized SNVs a) F1, B) F4 and c) F14.

4.2. Morphological characteristics of the optimized formulae

4.2.1. Transmission electron microscopy (TEM)

TEM images of the optimized (F1, F4, and F14), are shown in (Fig. 2a, b, and c). The nanospanlastic vesicles are homogeneous, well-defined, and have distinct spherical boundaries. This is because of the amphoteric nature of non-ionic surfactants, which causes the hydrophobic part to be oriented away from the aqueous environment, while the hydrophilic part maintains contact with it. The PS of the optimized formulae was found to agree with that measured previously.

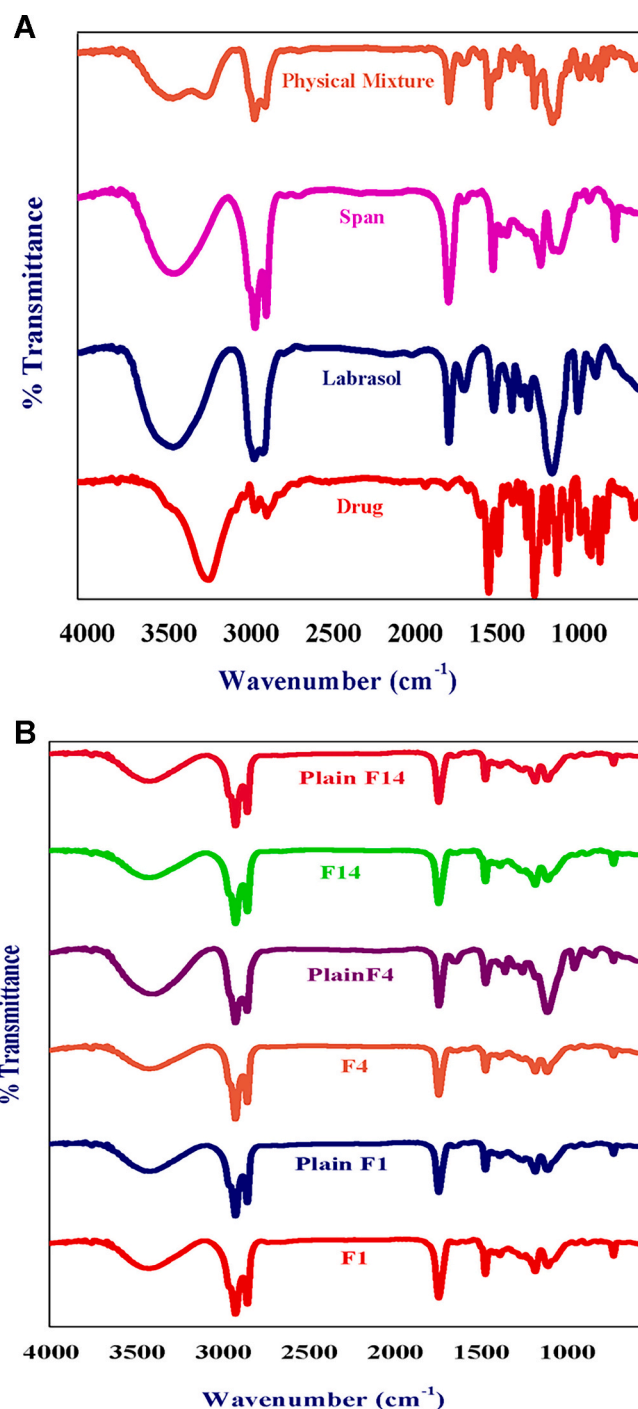


Fig. 3. A. FTIR of NBV, labrasol, span, and their physical mixture. B. FTIR of the optimized NBV-loaded SNVs F1, F4, and F14 and plain SNVs.

4.3. Solid characterization of the optimum SNVs

4.3.1. Fourier transform-infrared spectroscopy (FT-IR)

Fig. 3A represents FT-IR spectra of NBV, Span, labrasol, their PM, and the selected SNVs either plain or medicated. NBV spectrum showed two well-defined sharp bands at 3195 cm^{-1} , representing the stretching vibration of the hydroxyl group, at 2848 , 2920 , and 2985 cm^{-1} due to the C—H stretching, at 1622 cm^{-1} , 1564 cm^{-1} due to C=C stretching, 1303 cm^{-1} due to C—N stretching and at 1140 cm^{-1} due to C—O stretching (Vijayanand et al., 2016). As shown in this Figure, Labrasol exhibited a C—H stretching band at 2924 and 2870 cm^{-1} , C=O stretching at 1736 cm^{-1} , and broad peaks at 1108 due to C—O stretching (Karataş and Bekmezci, 2013).

Moreover, sharp and broad peaks at 2919 , 1739 , and 2850 cm^{-1} due to strong aromatic —CH₃ group, strong C = O ester bond, and OH group respectively in span 60 spectrum, and small peaks in the range of 1065 – 1178 cm^{-1} were due to aliphatic structure (Afreen et al., 2022).

FT-IR spectra of NBV-Labrasol-Span PM exhibited absorption peaks similar to those of NBV, Labrasol, and Span PM. This ruled out the possibility of the interaction between NBV and polymers used following physical mixing. In addition, FT-IR analysis is important for quick and efficient identification of encapsulated chemical molecules. In FT-IR spectra of NBV-SNVs, the disappearance of peaks related to the drug, may indicate the drug entrapment within SNVs and indicate no significant interaction between the drug and other ingredients (Fig. 3B).

4.3.2. Differential scanning calorimetry (DSC)

Fig. 4A depicts the differential scanning calorimetry (DSC) thermograms for NBV, Span, Labrasol, their PM, and the selected SNVs either plain or medicated. NBV thermogram showed a single sharp endothermic peak at $226.52\text{ }^{\circ}\text{C}$ (Trivedi et al., 2020). The drug's crystalline structure was revealed by its distinct peak and it corresponded to its melting point. Span 60 has an endothermic peak at $54.53\text{ }^{\circ}\text{C}$, which is its transition temperature. (Mohammed et al., 2023a).

Labrasol depicted two endothermic peaks at 301.20 and $404.05\text{ }^{\circ}\text{C}$. Thermograms of PM showed endothermic peaks from both the polymers and the drug, however, the intensity of both peaks was diminished likely due to the diluting effect. Since the drug could potentially disperse in the polymer's molten mass, the drug's peak was shifted to a lower temperature. Both the drug endotherms, span, and labrasol endothermic peak at 204.99 , 54.77 , 300.59 , $410.89\text{ }^{\circ}\text{C}$ respectively were present in the thermogram of their PM.

The absence of the endothermic peak of NBV in case of medicated SNVs might be attributed to its entrapment in the studied medicated SNVs (Fig. 4B)A. Consequently, the endotherm of the medicated SNVs was similar to that of the plain SNVs.

4.4. In vitro release of the optimized SNVs

Fig. 5 displays the release profile of NBV from a control suspension and the optimized three formulae (F1, F4, and F14). It was obvious that incorporating NBV within SNVs significantly slowed down the drug release as the vesicular system is well-known to act as a reservoir that slowly releases the drug providing a sustained release profile (Trivedi et al., 2020).

The percentage of NBV released from the suspension was $93.95 \pm 1.21\%$, within 5 h while SNVs showed a sustained release profile of NBV. This was in agreement with a previous study (Al-Shoubki et al., 2023b) that demonstrated that sodium valproate-loaded Spanlastics exhibited a more protracted drug release than the free drug.

Regarding the optimized SNVs (F1, F4, and F14), the drug release percentages were $90.14 \pm 1.30\%$, 82.50 ± 1.08 , and $85.47 \pm 0.55\%$ respectively after 12 h. F1 achieved the highest % drug released, but F4 has the lowest % as it has the highest EA% relative to the other optimized formulae. These results are in accordance with El Zaafarany et al. (El Zaafarany et al., 2010) who reported that drug release decreased

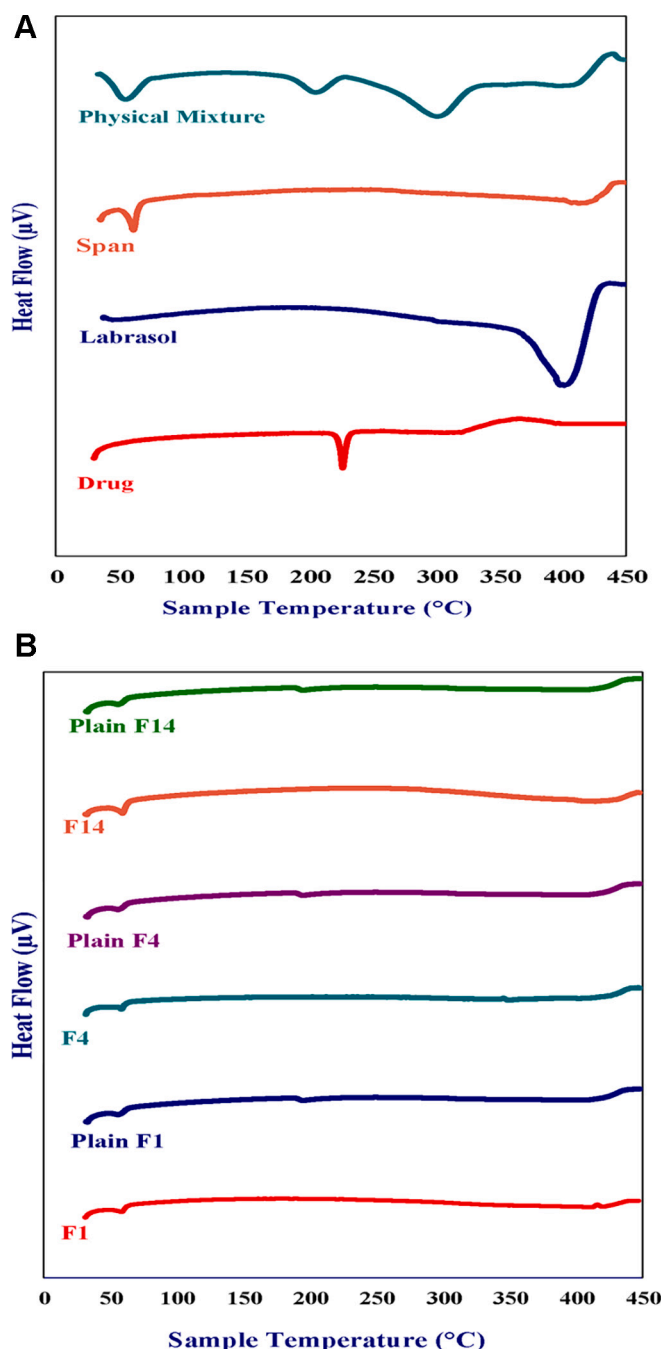


Fig. 4. A. DSC thermograms of NBV, Span, labrasol, and their PM. B. DSC thermograms of F1, F4, F14 and the plain SNVs.

upon increasing the amount of EA, due to the formation of mixed micelles that were less sensitive to concentration gradient than the vesicles. One possible explanation is that the NBV is being more effectively entrapped within the SNVs.

4.5. Statistical analysis

The release kinetics of NBV from the optimized formulations are presented in Table 5. The formulations followed the Higuchi diffusion model, based on kinetic study. Higuchi model posits that the process of drug release is facilitated by the diffusion of the drug through diffused vesicles. According to the model, it is proposed that the initial drug loading within the matrix surpasses its solubility in the surrounding media, resulting in a sink condition at the particles' wall. This

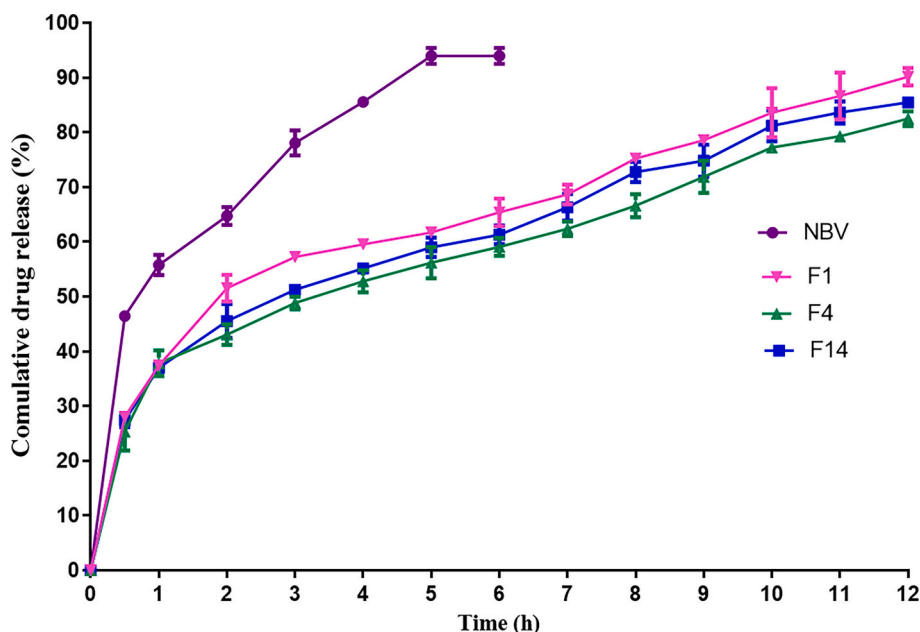


Fig. 5. In-vitro release of NBV at STF pH 7.4 (up to 12 h) from NBV suspension and the optimized NBV-loaded SNVs.

Table 5

Kinetic analysis of drug release data for optimized NBV-loaded SNVs.

Formula	Correlation coefficient (r^2)			
	Zero order	First order	Higuchi model	Korsmeyer-peppas R^2 n
F1	0.9421	0.9603	0.9800	0.9837 0.34
F4	0.9649	0.9771	0.9840	0.9784 0.34
F14	0.9671	0.9797	0.9905	0.9891 0.35

phenomenon facilitates the uniform and regulated diffusion of the medication inside the medium of release. As stated by (Paul, 2011) the utilization of the Korsmeyer-Peppas model reveals that the release pattern of NBV from the optimized formulations follows Fickian

Table 6

Effect of the different storage conditions on the physicochemical properties of the optimized SNVs.

	Freshly prepared	After 3 months of storage at 25 °C	After 3 months of storage at 4 °C
F1			
PS (nm)	411.66 ± 23.40	447.33 ± 86.83	434.30 ± 79.46
ZP (mV)	-33.90 ± 3.96	-32.75 ± 0.35	-32.45 ± 6.15
EE%	58.66 ± 1.10	51.80 ± 0.61	56.93 ± 0.18
F4			
PS (nm)	274.56 ± 13.65	317.80 ± 20.69	357.80 ± 24.04
ZP (mV)	-26.15 ± 0.45	-32.65 ± 0.25	-35.45 ± 1.65
EE%	50.22 ± 0.50	46.81 ± 0.82	48.18 ± 1.70
F14			
PS (nm)	256.63 ± 6.96	352.4 ± 24.00	237.83 ± 9.95
ZP (mV)	-27.66 ± 0.74	-23.03 ± 0.44	-32.7 ± 0.30
EE%	55.92 ± 0.82	53.84 ± 1.67	53.63 ± 2.11

transport, as seen by the presence of n values below 0.5.

4.6. Stability study

Table 6 illustrated the PS, ZP, and EE% of F1, F4, and F14 during storage for three months at room temperature (25 ± 1 °C), and in the refrigerator (4 ± 1 °C). After storage for three months, the optimized formulae F1, F4, and F14 showed no alterations in their appearance when subjected to various storage conditions. At zero-time, PS was 411.66 ± 23.40 , 274.56 ± 13.65 , and 256.63 ± 6.96 nm respectively, which non-significantly increased to 447.33 ± 86.83 , 317.80 ± 20.69 , and 352.4 ± 24.00 nm at room temperature by the end of the experiment ($P < 0.05$) which might be attributed to particle fusion during storage. The initial ZP for F1, F4, and F14 was -33.90 ± 3.96 , -26.15 ± 0.45 , and -27.66 ± 0.74 mV respectively at zero time. ZP non-significantly changed to -32.75 ± 0.35 , -32.65 ± 0.25 , and -23.03 ± 0.44 mV respectively at room temperature. Whereas, F1 and F4 EE% significantly decreased from 58.66 ± 1.10 and 50.22 ± 0.50 to 51.80 ± 0.61 and 48.18 ± 1.70 . That may be attributed to the release of NBV from the SNVs, caused by the concentration gradient between the SNVs and the surrounding aqueous medium (Alaeldin et al., 2021). However, F14 EE% non-significantly decreased from $55.92 \pm 0.82\%$ to $53.84 \pm 1.67\%$ during the storage period.

In contrast, the PS of F1, F4 and F14 reached 434.30 ± 79.46 , 357.80 ± 24.04 , and 237.83 ± 9.95 nm respectively by the third month at the refrigerator. The ZP was insignificantly changed to reach -32.45 ± 6.15 , -35.45 ± 1.65 , and -32.7 ± 0.30 mV. The high zeta potential may have hindered the aggregation and fusion of vesicles during storage (Agha et al., 2023). The EE% of the optimized F1, F4, and F14 decreased from 58.66 ± 1.10 , 50.22 ± 0.50 and $55.92 \pm 0.82\%$ to 56.93 ± 0.18 , 48.18 ± 1.70 and $53.63 \pm 2.11\%$, yet the difference was non-significant ($P < 0.05$). These findings indicated that the optimized formulae F1, F4 and F14 exhibited greater stability at refrigerator temperature, hence maintaining their efficacy for an extended duration during storage.

4.7. Compatibility study

Examining the intermolecular interactions among different components of a formulation is crucial to verifying their chemical compatibility (Abdeltawab et al., 2021) To investigate the chemical compatibility

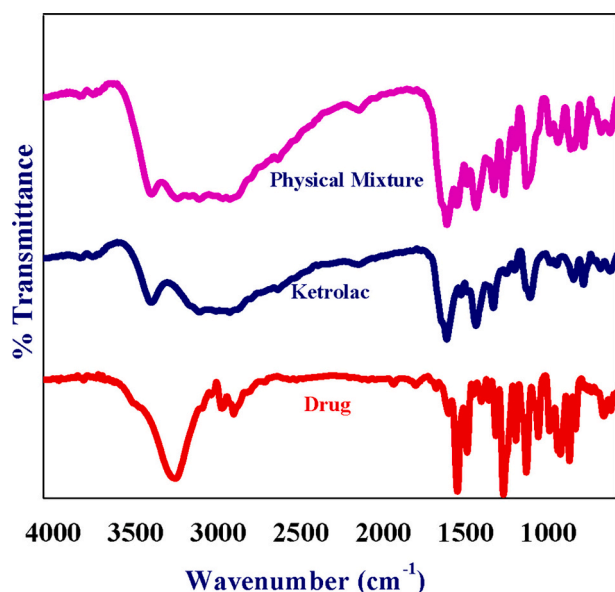


Fig. 6. FTIR of NBV, KET, and their physical mixture.

between KET and NBV, the FTIR spectrum of their mixture was compared to their spectra. As presented in Fig. 6, KET, NBV individually or their physical mixture triggered a shifting of their characteristic peaks. Yet, all characteristic peaks were preserved, suggesting the chemical compatibility between them.

The FTIR spectrum of ketorolac tromethamine exhibited principal peaks at 3346 cm^{-1} due to N—H and NH₂ stretching and the peak at 1380 cm^{-1} is due to —C—N vibrations, the peak at 1052 cm^{-1} is due to —OH bending confirms the presence of the alcoholic group (Suhail et al., 2021), while the peak at 1195 cm^{-1} (C=O) indicates stretch (di-aryl ketone). Peaks at 729 cm^{-1} , and 789 cm^{-1} confirm C—H bending (Aromatic) thus confirming the structure of ketorolac tromethamine.

FTIR spectrum of KET and NBV was compared to their physical mixture spectra. KET exhibited a shift of its N—H stretching from 3346 cm^{-1} to 3344 cm^{-1} , and NH₂ stretching. The peak at 1380 cm^{-1} is due to —C—N vibrations which show no clear difference between it and the physical mixture.

KET showed a shift of peak due to —OH bending confirming the presence of the alcoholic group at 1052 cm^{-1} to 1077 cm^{-1} . The peak at 1195 cm^{-1} (C=O) indicates stretch (di-aryl ketone) showed a shift to 1142 cm^{-1} . Peaks at 729 cm^{-1} , and 789 cm^{-1} confirming C—H bending (Aromatic) thus confirming the structure of ketorolac tromethamine exhibited a shift at 728 and 787 cm^{-1} .

whereas NBV showed a shift of its hydroxyl group (O—H) from 3195 to 3188 cm^{-1} due to hydrogen bonding, peaks at 2848 , 2920 , and 2985 cm^{-1} due to the C—H stretching exhibited a shift to 2871 , 3057 cm^{-1} , peak at 1564 cm^{-1} due to C=C stretching exhibited a shift to 1567 cm^{-1} , and at 1140 cm^{-1} due to C—O stretching to 1142 cm^{-1} due to hydrogen bonding. Yet, all characteristic peaks were preserved, suggesting the chemical compatibility between the two drugs.

Table 7

Physical properties of the prepared NBV-loaded SNVs and KET gel.

Formula	Appearance	Color	Homogeneity	Precipitation	PH	Drug content	Tsol-gel temp. (°C)	Tsol-gel time (min)
G1	Gel	Transparent	Homogenous	-ve	6.73 ± 0.33	98.75 ± 03	34 ± 0.22	0.43 ± 0.21
G2	Gel	Transparent	Homogenous	-ve	7.36 ± 0.23	99.46 ± 0.43	43 ± 0.21	2.32 ± 0.32
G3	Gel	Transparent	Homogenous	-ve	7.19 ± 0.07	94.63 ± 0.54	30 ± 0.33	2.38 ± 0.35
G4	Gel	Transparent	Homogenous	-ve	6.92 ± 0.03	93.42 ± 0.33	36 ± 0.11	0.27 ± 0.42
G5	Gel	Transparent	Homogenous	-ve	7.04 ± 0.26	91.43 ± 0.65	41 ± 0.01	2.45 ± 1.2
G6	Gel	Transparent	Homogenous	-ve	7.45 ± 0.44	96.33 ± 0.12	37 ± 0.9	0.23 ± 1.2

4.8. Evaluation of the prepared NBV-loaded SNVs and KET gel formulae

4.8.1. Visual inspection

The physical properties of the prepared NBV-loaded SNVs and KET gel formulae are displayed in Table 7. Regarding all formulations, the results disclosed no color change and no precipitation. Each formula was uniform, transparent, and colorless.

4.8.2. PH evaluation

As shown in Table 7, All tested formulae were discovered to have pH values between 6.73 ± 0.33 and 7.45 ± 0.44 . These values are considered acceptable and non-irritating for ocular administration (Lu et al., 2013).

4.8.3. Drug content evaluation

Drug content is considered an indicator for drug uniformity in any pharmaceutical dosage form. In accordance with the USP pharmacopeia, as shown in Table 6, the drug content of all of the developed formulations varied between 91.43 ± 0.65 and 99.46 ± 0.43 which means drug contents were in the acceptable range.

4.8.4. Sol-gel transition temperature (Tsol-gel) and gelation time

Tsol-gel is the temperature at which solutions gel. The physiological temperature of the ocular determines the sol-gel transition temperature range and time restrictions for ocular in situ gel delivery. Optimal formulas gel at $34\text{--}37\text{ }^{\circ}\text{C}$ ocular temperature. All formulations of Tsol-gel have a temperature range of 30 ± 0.33 to $43 \pm 0.21\text{ }^{\circ}\text{C}$ (Table 7). All formulations with 12% pluronic F127 and 2% and 4% HPMC showed Tsol-gel above $30\text{ }^{\circ}\text{C}$. Formulations F2 and F4 lower temperatures promote solvation and hydrogen bonding. In aqueous solutions at low temperatures, a hydration layer forms around pluronic F127 molecules due to hydrogen bonding between polymer chains and water molecules. Hydrogen bonds rupture at higher temperatures, desolvating polymer hydrophilic chains. This promotes hydrophobic polyoxypropylene domain contacts and gel formation. Even though HPMC is not thermoreversible, its addition as a mucoadhesive polymer lowered gelation temperature. Entanglement of HPMC long chains with pluronic F127 or hydrogen bonding at polymer chain contact points may decrease gelation. Gelation time for all formulations was $0.23 \pm 1.2\text{--}2.38 \pm 0.35$ min. Since pluronic F127 is a thermoreversible polymer, gelation occurs owing to solubility profile changes, and higher HPMC concentrations accelerated gelling. However, all formulations gelled within 2.38 min, showing good gel formation. Therefore, mucociliary clearance could not expel the formulation.

4.8.5. Rheological study

Table 8 illustrates the rheological data of NBV-loaded SNVs and KET gel. All formulae were found to exhibit non-Newtonian shear thinning (pseudo-plastic) flow, as the viscosity decreased the shear rate increased. According to (Lee et al., 2009) pseudoplastic flow may be caused by the progressive rupture of the formulation's internal structure (due to increasing shear) and its subsequent reconstruction via Brownian movement. The characteristics of shear-thinning are highly advantageous for topical preparations as they ensure that they exhibit a thin consistency during application while becoming thicker under other

Table 8

Rheological data of NBV-loaded SNVs and KET gel formulae.

Formula	η min (cps)	η max (cps)	Hysteresis area(cm ²)	Farrow's constant(N)	Flow index (n)	Flow behavior
G1	1900	4140	3.00	1.40	0.71	pseudoplastic flow (shear rate thinning)
G2	7420	25,000	5.76	1.78	0.55	pseudoplastic flow (shear rate thinning)
G3	1590	3070	1.00	1.30	0.77	pseudoplastic flow (shear rate thinning)
G4	5670	15,500	2.30	1.60	0.62	pseudoplastic flow (shear rate thinning)
G5	2410	5730	1.94	1.47	0.68	pseudoplastic flow (shear rate thinning)
G6	4170	12,100	2.01	1.66	0.60	pseudoplastic flow (shear rate thinning)

conditions (Abdelmonem et al., 2021).

Clearly, the Farrow constant (N) is >1 for all formulae indicating non-Newtonian shear-thinning pseudoplastic flow behavior. As indicated by the results. The flow index (n) values were <1 according to the power law upon increasing polymer concentration revealing a non-Newtonian shear-thinning pseudoplastic behavior as illustrated in Table 8. The lower the value of n, the more shear-thinning the formulation is (Chang et al., 2002). Table 7 illustrates a significant increase in viscosity at both η max (viscosity at the maximum shear rate) and η min (viscosity at the minimum shear rate) as the polymer content is increased (Fang et al., 2003).

4.8.6. In-vitro release of NBV from NBV SNVs- KET-loaded gel

Fig. 7 demonstrates the in vitro release profiles of NBV from the prepared gel formulae (G1, G2, G3, G4, G5, and G6) corresponding to NBV gel. The in vitro release from the gel formulations up to 12 h was more sustained than that from the conventional NBV gel formula that exhibited $96.37 \pm 3.78\%$ drug released after 4 h and 96.71 ± 2.15 after 6 h in gel containing 2% and 4% W/W HPMC respectively. That could be interpreted based on better entrapment of NBV within the SNVs.

After 12 h, the drug release from G1, G3, and G5 formulations containing 2% w/w HPMC was $76.36 \pm 0.90\%$, 71.63 ± 1.09 , and $70.79 \pm 3.12\%$, respectively. Drug release was seen to be $62.58 \pm 0.90\%$, $59.66 \pm 0.91\%$, and $61.99 \pm 0.68\%$ after 12 h in the G2, G4, and G6 formulations containing 4% w/w HPMC, respectively. The bursting effect caused a sudden increase in drug release from these formulations, but the gelation effect happens, slowing the release rate.

Compared to G2, G4, and G6, the release from formulations G1, G3, and G5 was much greater. The greater gelation capacity and viscosity of the 4% HPMC formulation was attributed to the difference between it

and the 2% HPMC formulations. It's possible that HPMC significantly delays the drug release probably by delaying the polymer disintegration (Güven et al., 2019). All of the prepared formulations showed delayed and prolonged release properties in comparison to NBV gel. G1 was selected as the optimum formula as it exhibited the highest release % of NBV up to 12 h.

4.9. Ex-vivo visualization of the ocular using CLSM

Fig. 8 shows CLSM images of the rabbit ocular tissue showing RhB uptake of its RhB solution, RhB-loaded drug solution, RhB-loaded SNVs, and RhB-loaded SNVs gel. After applying the previous formulation topically, When RhB-loaded SNVs gel and RhB-loaded SNVs are administered to the eye instead of Rh solution or RhB-loaded medication solution, the increased fluorescence intensity in the eye is obviously seen (Fig. 8a, b, c, and d). This shows enhanced dye penetration. Because of their good physicochemical features and biocompatibility, surfactants found in spanlastic have shown to be essential in medication delivery. Spastics have long demonstrated their ability to improve medication absorption through the eyes. Their primary advantage is that they can increase the permeability and bioavailability of medications by making it easier for the drugs to pass through the membrane and by making the membrane more fluid and permeable. Additionally, they support medication absorption through transporter-mediated mechanisms. Rabbits given RhB solution had poor fluorescence intensity in their ocular tissues (Elhabal et al., 2023). Its rapid clearance and hydrophilic properties may be connected to this. This result confirms that the SNV is appropriate for treating ocular glaucoma and inflammation since it can distribute the drugs to the right place efficiently.

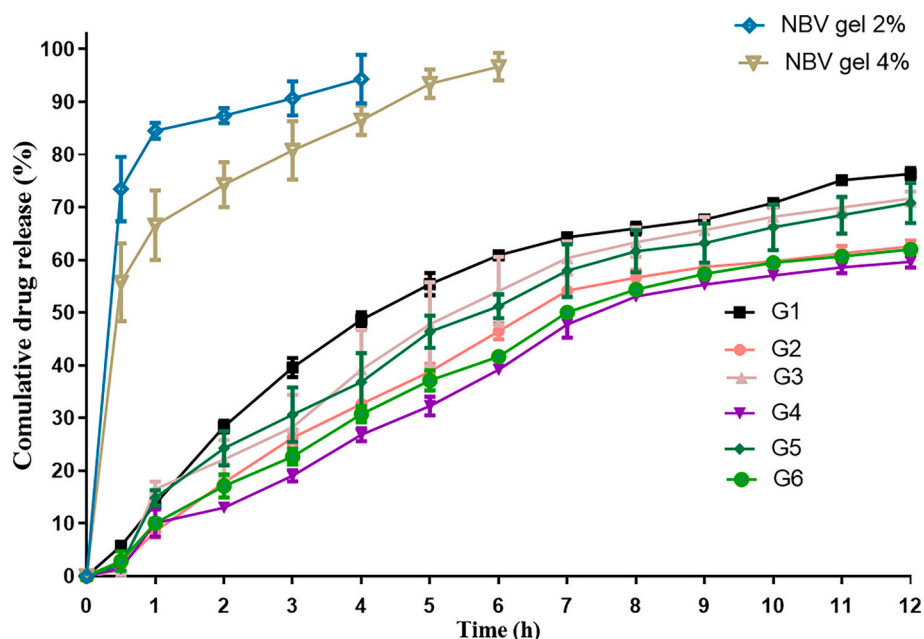


Fig. 7. In-vitro release of NBV at STF pH 7.4 (12h) from prepared NBV-loaded SNVs and KET Gel formulae.

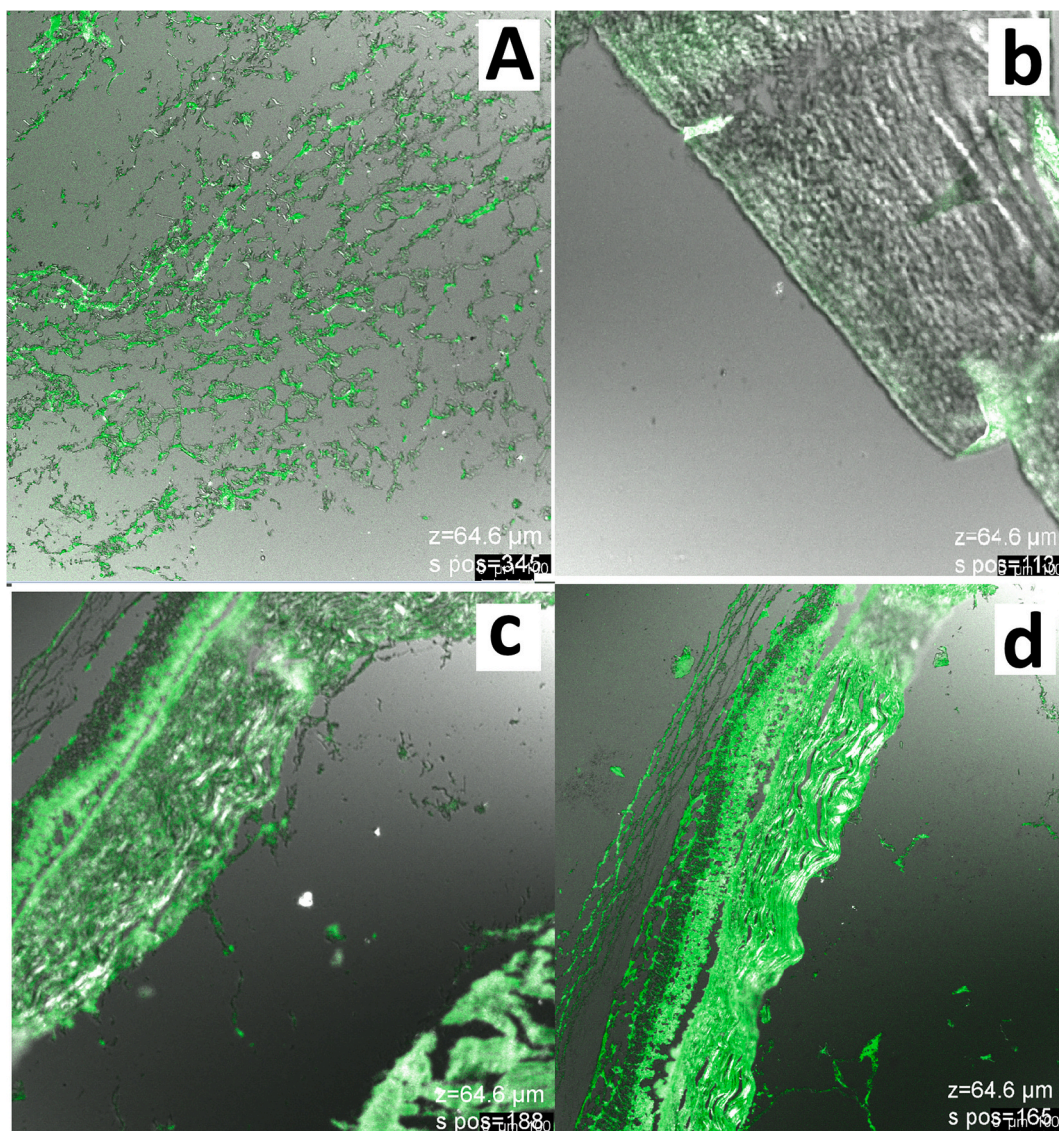


Fig. 8. Comparative CLSM images show the depth and intensity of Rhodamine B solution (A), RhB-loaded drug solution (B), RhB-loaded SNVs (C), and RhB-loaded SNVs gel(d).

4.10. In-vivo evaluation of NBV-loaded SNVs and KET gel

4.10.1. Ocular irritation study (Draize test)

After 21 days, an eye irritancy test was conducted, and the results showed that there were no inflammatory indications, such as redness, edema, or increased tear production. The ocular examination revealed a clean and flat cornea, normal conjunctiva and iris, a regular and reactive pupil, and a formed clear anterior chamber (Abdelmonem et al., 2021). These findings support the safety of optimized NBV-loaded SNVs (F1) and NBV-loaded SNVs and KET in gel (G1) for topical administration to

Table 9

Pharmacokinetic characteristics of NBV in aqueous humor following ocular delivery.

Parameters	GP1	GP2	GP3	GP4
$t_{1/2}$ (h)	12.01 ± 0.51	11.99 ± 0.53	12.11 ± 0.32	11.58 ± 0.11
t_{max} (h)	2.64 ± 1.21	2.35 ± 0.94	5.01 ± 1.03	6.01 ± 1.10
C_{max} (μg/mL)	1.84 ± 0.12	2.51 ± 0.32	5.01 ± 0.25	6.25 ± 0.35
AUC (0-8) (μg h/mL)	24.99 ± 1.02	22.54 ± 0.13	50.15 ± 0.72	65.14 ± 1.33

the eye.

4.10.2. Pharmacokinetic study

Pharmacokinetic characteristics and concentration-time profiles of drugs after a single installation are given in Table 9 and Fig. 9. The results illustrated that (GP4) administered NBV- loaded SNVs and KET ocugel has the highest C_{max} 6.25 ± 0.35 μg/mL, t_{max} 6.01 ± 1.10 h and AUC (0–8 h) 65.14 ± 1.33 μg h/mL when compared to GP1, GP2 and GP3 which showed C_{max} (1.84 ± 0.12, 2.51 ± 0.32 and 5.01 ± 0.25 μg/mL, respectively), t_{max} (2.63 ± 1.21, 2.35 ± 0.94 and 5.01 ± 1.03 h, respectively) and AUC (0-8 h) (24.99 ± 1.02, 22.54 ± 0.13 and 50.15 ± 0.72 μg h/mL, respectively) indicating a higher drug bioavailability than other groups which was 2.43 times longer than that of GP 1 which received NBV suspension. These findings aligned with the higher trans-corneal permeability combination and their gel in comparison to the solution. Based on the results of the pharmacokinetic analysis, it can be concluded that the combination gel successfully increased the bioavailability of NBV and KET by extending their retention time. Similar findings were found by Ban et al. (Ban et al., 2017) who showed the effect of the encapsulation of the drug into nanoparticles on drug pharmacokinetics in aqueous humor whereas Abdelmonem et al.

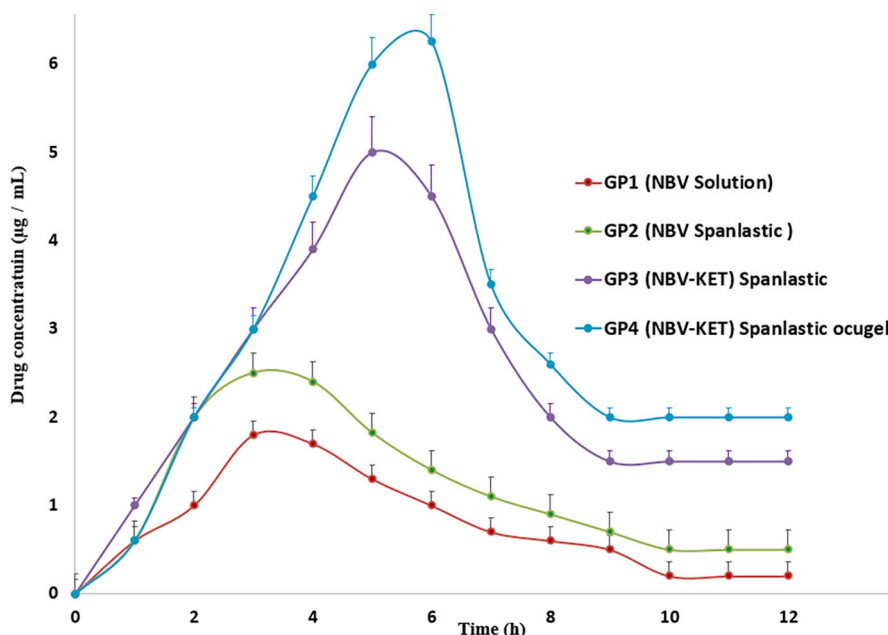


Fig. 9. Pharmacokinetic characteristics and concentration-time profiles of drugs after a single installation.

compared the ocular bioavailability of Acetazolamide and carvedilol aqueous solution with that of a combination of the two drugs, finding that the noisome charged lipid nanoparticle revealed higher drug retention time and enhanced drug permeation to the cornea (Abdelmonem et al., 2021).

4.10.3. Pharmacodynamic study (IOP measurement)

There were four sets of six albino rabbits from New Zealand. For two days in a row, the typical ocular pressure of 20.80 ± 24.90 mmHg was measured. After 3 weeks of dexamethasone injection into the anterior chamber, the IOP rose to about 40 mmHg. The right eye's IOP for each rabbit in each group stayed above 40 mmHg during the measuring time, indicating no systemic medication absorption. Following the administration of NBV-loaded SNVs (F1) in combination with KET as a solution and NBV-loaded SNVs (F1) and KET gel (GP3 and GP4), the IOP in each

rabbit reduced to normal (25.35 ± 1.01 mmHg and 21.25 ± 1.54 mmHg, respectively), remained within the normal range for twenty-four hours, and subsequently gradually rose, as shown in (Fig. 10). Following the IOP, the IOP for G3 was returned to normal after 30 min and remained within the normal range for 36 h. Instead of returning to normal after 1.30 h of treatment with (GP4) NBV-loaded SNVs and KET ocugel (G1), IOP was maintained within the normal range for 48 h before gradually rising. In comparison to its solution, the gel formulation exhibits a shorter t_{max} and longer retention duration. At the 48-h intervals, the percentage IOP reduction between groups 3–4 and the other groups was statistically significant ($P < 0.05$). This validated the long-lasting impact.

4.10.4. Histological examination

Examining the cornea, filtration angle, choroid, and retina was

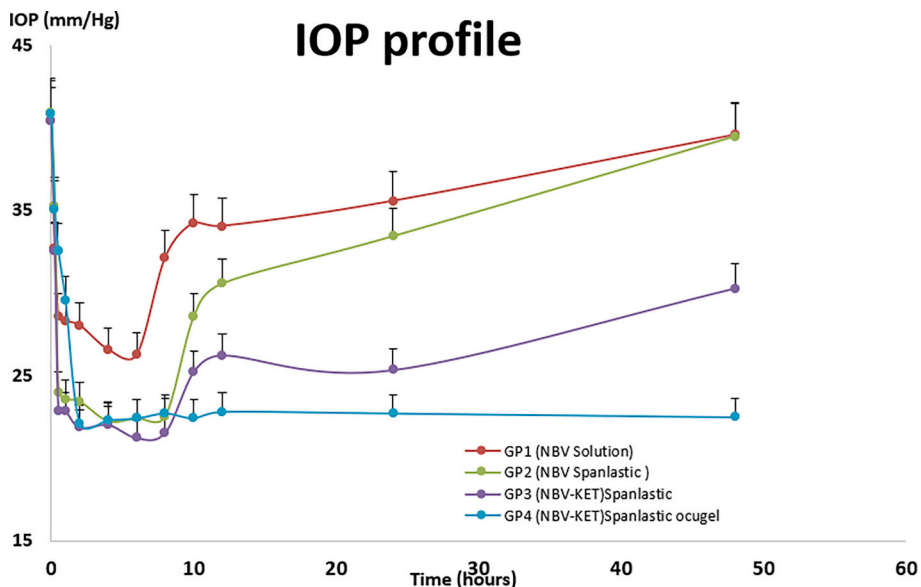


Fig. 10. Mean IOP of hypertensive rabbits for first 48 h with a certain administration compared to physiological minimum IOP for rabbit (IOP lower limit) and physiological maximum (IOP upper limit).

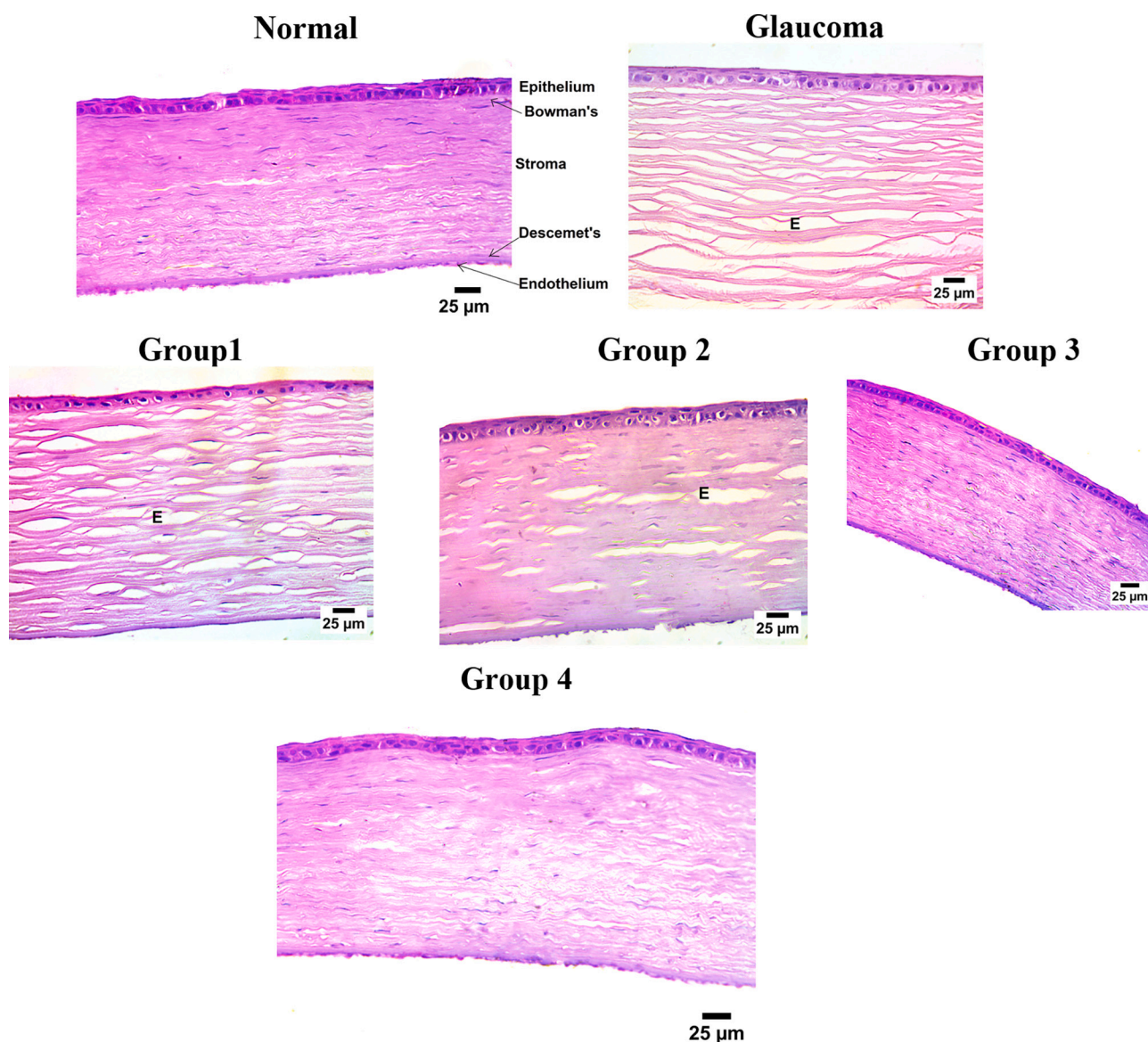


Fig. 11. Photomicrographs of the cornea (H&E). Where normal group exhibited histologically normal cornea, the glaucoma group displayed marked corneal stromal edema, Group 1 revealed moderate edema, Group 2 represented mild edema cornea, and Groups 3, and 4 showed normal cornea.

included in a microscopic examination of the eye's tissue. In Fig. 11, we observe that the corneas of the sham-operated controls had a typical five-layer histological arrangement (from outer to inner): non-keratinized squamous epithelium; epithelial basement membrane; corneal stroma; Descemet's membrane; endothelium. Extreme corneal edema, with edematous fluid spreading across the corneal stroma, was observed in the glaucoma group. Mild corneal edema was seen in Groups 3 (combination of KET and optimum NBV-loaded SNVs, F1) and GP4 (optimal combination of KET and NBV-loaded SNVs gel, G1), indicating that treatment with the various formulations reduced corneal damage. Group 2 (optimum NBV-loaded SNVs, F1) resulted in a significantly improved cornea; Group 1 (NBV-Solution) exhibited moderate corneal edema.

Concerning the filtration apparatus, in the normal group, the irido-corneal angle contained a normally appearing trabecular meshwork that is responsible for the drainage of aqueous humor and the ciliary body, a ring-shaped tissue located in the posterior ocular chamber that contains the ciliary muscle and a double layer of two, partly folded, neuro-epithelia, the non-pigmented, and the pigmented epithelium. Extensive histological changes in the filtration apparatus were seen in the

glaucomatous group, including basement membrane thickening of the ciliary body with increased deposition of collagen and hyalinises of ciliary muscles. Extracellular plaques were deposited, and the trabecular meshwork became hyalinized as cellular components were reduced and matrix and fibrillary components increased. Between the retina and the sclera lies a layer of blood vessels and connective tissue called the choroid. The normal group has normal choroid (Abdelmonem et al., 2021; Sammar Fathy Elhabal et al., 2023b). The choroid was compressed in those with glaucoma. Choroidal compression appeared mild in Group 2, and moderate in Group 1, whereas it was histologically normal in Group 3,4. Diffuse retinal atrophy and inner ganglion cell loss were seen in the glaucoma group, indicating retinal damage. The remaining ganglion cells were shrunken and hyperchromatic and their nuclei were pyknotic. Throughout the cell nucleus, both the inner and outer plexiform layers were thinned to varying degrees.

Multiple clear spherical gaps are typically detected in the inner plexiform layer of the retina in cases with microcystoid degeneration. Diffuse retinal thinning was seen in the Group 1 treatment group, while loss of ganglion cells and mild microcystin degeneration were observed in Group 2. Retina health was maintained in Groups 3 and 4.

5. Conclusions

Our results indicate a potential effect of Nebivolol as a beta-blocker for glaucoma with ketorolac as an anti-inflammatory for treatment complications of glaucoma, formulated by using a spanlastic formulation. Spanlastic prepared using the ethanol injection technique can enhance the permeability of NBV. The optimal formulation based on expert design Spanlastic made with Span 60 as a surfactant and 25% Labrasol as an edge activator, which decreases the eye's intraocular pressure rapidly and significantly. Combining NBV with KET has a synergistic impact in the treatment of glaucoma. The greatest outcomes are seen with SNVs gel and SNVS in combination with KET in gel due to increased bioavailability, proper release kinetics, and prolonged action of spanlastic gel in curing glaucoma. It can be concluded that the Combination of NBV-loaded SNVs and KET gel shows promise as a sustained-release formulation for the treatment of glaucoma, and may be utilized to improve patients' adherence to their medication regimens.

Institutional review board statement

The animal study protocol was approved by the animal care and use committee of the Faculty of Pharmacy, Cairo University, Cairo, Egypt (PI 2688 on 27/4/2020).

Informed consent statement

Not applicable.

Funding

This research received no external funding.

CRediT authorship contribution statement

Mohamed Yasser: Data curation, Investigation, Project administration. **Eman E. El Naggar:** Data curation, Investigation, Methodology. **Nehal Elfar:** Data curation, Methodology, Resources. **Mahmoud H. Teaima:** Supervision, Visualization, Writing – original draft. **Mohamed A. El-Nabarawi:** Formal analysis, Validation, Writing – review & editing. **Sammar Fathy Elhabal:** Conceptualization, Writing – original draft, Writing – review & editing.

Declaration of competing interest

The authors wish to declare no interest is involved in this publication.

Data availability

Data is contained within the article and supplementary materials.

Appendix A. Supplementary data

Supplementary data to this article can be found online at <https://doi.org/10.1016/j.ijpharm.2023.100228>.

References

Abdelbary, A.A., AbouGhaly, M.H.J.L.J.O.P., 2015. Design and optimization of topical methotrexate loaded niosomes for enhanced management of psoriasis: application of Box–Behnken design, in-vitro evaluation and in-vivo skin deposition study. *Int. J. Pharm.* 485, 235–243. <https://doi.org/10.1016/j.ijpharm.2015.03.020>.

Abdelmonem, R., Elhabal, S.F., Abdelmalak, N.S., El-Nabarawi, M.A., Teaima, M.H., 2021. Formulation and characterization of acetazolamide/carvedilol niosomal gel for glaucoma treatment: in vitro, and in vivo study. *Pharmaceutics* 13, 221. <https://doi.org/10.3390/pharmaceutics13020221>.

Abdeltawab, H., Svirskis, D., Boyd, B.J., Hill, A., Sharma, M., 2021. Injectable thermoresponsive gels offer sustained dual release of bupivacaine hydrochloride and

ketorolac tromethamine for up to two weeks. *Int. J. Pharm.* 604, 120748 <https://doi.org/10.1016/j.ijpharm.2021.120748>.

Afreen, U., Fahlelbom, K.M., Shah, S.N.H., Ashames, A., Almas, U., Khan, S.A., Yameen, M.A., Nisar, N., Asad, M.H.H.B., Murtaza, G., 2022. Formulation and evaluation of niosomes-based chlorpheniramine gel for the treatment of mild to moderate skin allergy. *J. Exp. Nanosci.* 17, 467–495. <https://doi.org/10.1080/17458080.2022.2094915>.

Agha, O.A., Girgis, G.N., El-Sokkary, M.M., Soliman, O.A.E.-A., 2023. Spanlastic-laden in situ gel as a promising approach for ocular delivery of Levofloxacin: in-vitro characterization, microbiological assessment, corneal permeability and in-vivo study. *Int. J. Pharm.*: X 6, 100201. <https://doi.org/10.1016/j.ijpx.2023.100201>.

Alaaeldin, E., Mostafa, M., Mansour, H.F., Soliman, G.M., 2021. Spanlastics as an efficient delivery system for the enhancement of thymoquinone anticancer efficacy: fabrication and cytotoxic studies against breast cancer cell lines. *J. Drug Deliv. Sci. Technol.* 65, 102725 <https://doi.org/10.1016/j.jddst.2021.102725>.

Ali, J., Bhatnagar, A., Kumar, N., Ali, A., 2014. Chitosan nanoparticles amplify the ocular hypotensive effect of catechol in rabbits. *Int. J. Biol. Macromol.* 65, 479–491. <https://doi.org/10.1016/j.ijbiomac.2014.02.002>.

Al-Shoubki, A.A., Teaima, M.H., Abdelmonem, R., El-Nabarawi, M.A., Elhabal, S.F., 2023a. Potential application of sucrose acetate isobutyrate, and glyceryl monooleate for nanonization and bioavailability enhancement of rivaroxaban tablets. *Pharm. Sci. Adv.* 100015. <https://doi.org/10.1016/J.PSCIA.2023.100015>.

Al-Shoubki, A.A., Teaima, M.H., Abdelmonem, R., El-Nabarawi, M.A., Elhabal, S.F., 2023b. Sucrose acetate isobutyrate (SAIB) and glyceryl monooleate (GMO) hybrid nanoparticles for bioavailability enhancement of rivaroxaban: an optimization study. *Pharm. Dev. Technol.* 1–11. <https://doi.org/10.1080/10837450.2023.2274944>.

Ammar, H.O., Salama, H., Ghorab, M., Mahmoud, A., 2009. Nanoemulsion as a potential ophthalmic delivery system for dorzolamide hydrochloride. *AAPS PharmSciTech* 10, 808–819. <https://doi.org/10.1208/s12249-009-9268-4>.

Ansari, M.D., Saifi, Z., Pandit, J., Khan, I., Solanki, P., Sultana, Y., Aqil, M.J.A.P., 2022. Spanlastics a novel nanovesicular carrier: its potential application and emerging trends in therapeutic delivery. *AAPS PharmSciTech* 23, 112. <https://doi.org/10.1208/s12249-022-02217-9>.

Badria, F.A., Abdelaziz, A.E., Hassan, A.H., Elgazar, A.A., Mazyed, E.A., 2020. Development of provesicular nanodelivery system of curcumin as a safe and effective antiviral agent: statistical optimization, in vitro characterization, and antiviral effectiveness. *Molecules* 25, 5668. <https://doi.org/10.3390/molecules25235668>.

Bakhaidar, R.B., Hosny, K.M., Mahier, I.M., Rizq, W.Y., Safhi, A.Y., Bukhary, D.M., Sultan, M.H., Bukhary, H.A., Madkhali, O.A., Sabei, F.Y., 2022. Development and optimization of a tamsulosin nanostructured lipid carrier loaded with saw palmetto oil and pumpkin seed oil for treatment of benign prostatic hyperplasia. *Drug Deliv.* 29, 2579–2591. <https://doi.org/10.1080/10717544.2022.2105448>.

Ban, J., Zhang, Y., Huang, X., Deng, G., Hou, D., Chen, Y., Lu, Z., 2017. Corneal permeation properties of a charged lipid nanoparticle carrier containing dexamethasone. *Int. J. Nanomedicine* 1329–1339. <https://doi.org/10.2147/IJN.S126199>.

Bancroft, J.D.S.T.D.R., 2013. *Theory and Practice of Histological Techniques*, 7th ed.; ed. Churchill Livingstone Elsevier, London, UK.

Basalious, E.B., Shawky, N., Badr-Eldin, S.M., 2010. SNEDDS containing bioenhancers for improvement of dissolution and oral absorption of lacidipine. I: development and optimization. *Int. J. Pharm.* 391, 203–211. <https://doi.org/10.1016/j.ijpharm.2010.03.008>.

Baudouin, C., Kolko, M., Melik-Parsadaniantz, S., Messmer, E.M., 2021. Inflammation in glaucoma: from the back to the front of the eye, and beyond. *Prog. Retin. Eye Res.* 83, 100916 <https://doi.org/10.1016/j.preteyeres.2020.100916>.

Bessone, C.D.V., Akhlaghi, S.P., Tártara, L.I., Quinteros, D.A., Loh, W., Allemanni, D.A., 2021. Latanoprost-loaded phytantriol cubosomes for the treatment of glaucoma. *Eur. J. Pharm. Sci.* 160, 105748 <https://doi.org/10.1016/j.ejps.2021.105748>.

Chang, J.Y., Oh, Y.-K., Choi, H.-G., Kim, Y.B., Kim, C.-K., 2002. Rheological evaluation of the thermosensitive and mucoadhesive vaginal gels in physiological conditions. *Int. J. Pharm.* 241, 155–163. [https://doi.org/10.1016/S0378-5173\(02\)00232-6](https://doi.org/10.1016/S0378-5173(02)00232-6).

Das, B., Sen, S.O., Maji, R., Nayak, A.K., Sen, K.K., 2017. Transfersomal gel for transdermal delivery of risperidone: formulation optimization and ex vivo permeation. *J. Drug Deliv. Sci. Technol.* 38, 59–71. <https://doi.org/10.1016/j.jddst.2017.01.006>.

Das, B., Nayak, A.K., Mallick, S., 2022. Lipid-based nanocarriers for ocular drug delivery: an updated review. *J. Drug Deliv. Sci. Technol.* 103780. <https://doi.org/10.1016/j.jddst.2022.103780>.

Draize, J.H., 1944. Methods for the study of irritation and toxicity of substances applied topically to the skin and the mucous membranes. *J. Pharmacol. Exp. Ther.* 82, 377–390.

Duangjit, S., Opanasopit, P., Rojanarata, T., Ngawhirunpat, T., 2013. Evaluation of meloxicam-loaded cationic transfersomes as transdermal drug delivery carriers. *AAPS PharmSciTech* 14, 133–140. <https://doi.org/10.1208/s12249-012-9904-2>.

El Zaafarany, G.M., Awad, G.A., Holayel, S.M., Mortada, N.D., 2010. Role of edge activators and surface charge in developing ultra-deformable vesicles with enhanced skin delivery. *Int. J. Pharm.* 397, 164–172. <https://doi.org/10.1016/j.ijpharm.2010.06.034>.

Elhabal, S.F., Elwy, H.M., Hassanin, S., El-Rashedy, A.A., Hamza, A.A., Khasawneh, M.A., 2022. Biosynthesis and characterization of gold and copper nanoparticles from salvadora persica fruit extracts and their biological properties. *Int. J. Nanomedicine* 17, 6095–6112. <https://doi.org/10.2147/IJN.S385543>.

Elhabal, S.F., Ghaffar, S.A., Hager, R., Elzohairy, N.A., Khalifa, M.M., Mohie, P.M., Gad, R.A., Omar, N.N., Elkomy, M.H., Khasawneh, M.A., 2023. Development of thermosensitive hydrogel of amphotericin-B and lactoferrin combination-loaded

- PLGA-PEG-PEI nanoparticles for potential eradication of ocular fungal infections: in vitro, ex-vivo and in-vivo studies. *Int. J. Pharm.*: X 5, 100174. <https://doi.org/10.1016/j.ijpharm.2023.100174>.
- ElMeshad, A.N., Mohsen, A.M., 2016. Enhanced corneal permeation and antimycotic activity of itraconazole against *Candida albicans* via a novel nanosystem vesicle. *Drug Deliv.* 23, 2115–2123. <https://doi.org/10.3109/10717544.2014.942811>.
- Elsherif, N.L., Shamma, R.N., Abdelbary, G., 2017. Terbinafine hydrochloride transungual delivery via nanovesicular systems: in vitro characterization and ex vivo evaluation. *AAPS PharmSciTech* 18, 551–562. <https://doi.org/10.1208/s12249-016-0528-9>.
- Esteban-Pérez, S., Andrés-Guerrero, V., López-Cano, J.J., Molina-Martínez, I., Herrero-Vanrell, R., Bravo-Osuna, I., 2020. Gelatin nanoparticles-HPMC hybrid system for effective ocular topical administration of antihypertensive agents. *Pharmaceutics* 12, 306. <https://doi.org/10.3390/pharmaceutics12040306>.
- Fahmy, A.M., El-Setouhy, D.A., Habib, B.A., Tayel, S.A., 2019. Enhancement of transdermal delivery of haloperidol via spanlastic dispersions: entrapment efficiency vs. particle size. *AAPS PharmSciTech* 20, 1–13. <https://doi.org/10.1208/s12249-019-1306-2>.
- Fang, J.-Y., Yu, S.-Y., Wu, P.-C., Huang, Y.-B., Tsai, Y.-H., 2001. In vitro skin permeation of estradiol from various proniosome formulations. *Int. J. Pharm.* 215, 91–99. [https://doi.org/10.1016/s0378-5173\(00\)00669-4](https://doi.org/10.1016/s0378-5173(00)00669-4).
- Fang, J.-Y., Hwang, T.-L., Leu, Y.-L., 2003. Effect of enhancers and retarders on percutaneous absorption of flurbiprofen from hydrogels. *Int. J. Pharm.* 250, 313–325. [https://doi.org/10.1016/s0378-5173\(02\)00540-9](https://doi.org/10.1016/s0378-5173(02)00540-9).
- Farghaly, D.A., Aboelwafa, A.A., Hamza, M.Y., Mohamed, M.I., 2017. Topical delivery of fenopropfen calcium via elastic nano-vesicular spanlastics: optimization using experimental design and in vivo evaluation. *AAPS PharmSciTech* 18, 2898–2909. <https://doi.org/10.1208/s12249-017-0771-8>.
- Gaafar, P.M., Abdallah, O.Y., Farid, R.M., Abdelkader, H., 2014. Preparation, characterization and evaluation of novel elastic nano-sized niosomes (ethniosomes) for ocular delivery of prednisolone. *J. Liposome Res.* 24, 204–215. <https://doi.org/10.3109/08982104.2014.881850>.
- Gaudana, R., Ananthula, H.K., Parenky, A., Mitra, A.K., 2010. Ocular drug delivery. *AAPS J.* 12, 348–360. <https://doi.org/10.1208/s12248-010-9183-3>.
- Güven, U.M., Berkman, M.S., Şenel, B., Yazan, Y., 2019. Development and in vitro/in vivo evaluation of thermo-sensitive in situ gelling systems for ocular allergy. *Braz. J. Pharm. Sci.* 55. <https://doi.org/10.1590/s2175-97902019000117511>.
- Hallan, S.S., Sguizzato, M., Mariani, P., Cortesi, R., Huang, N., Simelière, F., Marchetti, N., Drechsler, M., Ruzgas, T., Esposito, E., 2020. Design and characterization of ethosomes for transdermal delivery of caffeic acid. *Pharmaceutics* 12, 740. <https://doi.org/10.3390/pharmaceutics12080740>.
- Huang, J., Peng, T., Li, Y., Zhan, Z., Zeng, Y., Huang, Y., Pan, X., Wu, C.-Y., Wu, C., 2017. Ocular cubosome drug delivery system for timolol maleate: preparation, characterization, cytotoxicity, ex vivo, and in vivo evaluation. *AAPS PharmSciTech* 18, 2919–2926. <https://doi.org/10.1208/s12249-017-0763-8>.
- Ismail, A., Nasr, M., Sammour, O., 2020. Nanoemulsion as a feasible and biocompatible carrier for ocular delivery of travoprost: improved pharmacokinetic/ pharmacodynamic properties. *Int. J. Pharm.* 583, 119402. <https://doi.org/10.1016/j.ijpharm.2020.119402>.
- Jaafar-Maalej, C., Diab, R., Andrieu, V., Elaissari, A., Fessi, H., 2010. Ethanol injection method for hydrophilic and lipophilic drug-loaded liposome preparation. *J. Liposome Res.* 20, 228–243. <https://doi.org/10.3109/08982100903347923>.
- Jiang, J., Ma, T., Zhang, L., Cheng, X., Wang, C., 2020. The transdermal performance, pharmacokinetics, and anti-inflammatory pharmacodynamics evaluation of harmine-loaded ethosomes. *Drug Dev. Ind. Pharm.* 46, 101–108. <https://doi.org/10.1080/03639045.2019.1706549>.
- Kakkar, S., Kaur, I.P., 2011. Spanlastics—a novel nanovesicular carrier system for ocular delivery. *Int. J. Pharm.* 413, 202–210. <https://doi.org/10.1016/j.ijpharm.2011.04.027>.
- Karatás, A., Bekmezci, S., 2013. Evaluation and enhancement of physical stability of semi-solid dispersions containing piroxicam into hard gelatin capsules. *Acta Pol. Pharm.* 70, 883–897.
- Kaviarasi, B., Rajana, N., Pooja, Y.S., Rajalakshmi, A., Singh, S.B., Mehra, N.K., 2023. Investigating the effectiveness of difluprednate-loaded core-shell lipid-polymeric hybrid nanoparticles for ocular delivery. *Int. J. Pharm.* 640, 123006. <https://doi.org/10.1016/j.ijpharm.2023.123006>.
- Khallaf, A.M., El-Moslemany, R.M., Ahmed, M.F., Morsi, M.H., Khalafallah, N.M., 2022. Exploring a novel fasudil-phospholipid complex formulated as liposomal thermosensitive in situ gel for glaucoma. *Int. J. Nanomedicine* 163–181. <https://doi.org/10.2147/ijn.s342975>.
- Khan, N., Aqil, M., Ameeruzzafar, Imam, S.S., Ali, A., 2015. Development and evaluation of a novel in situ gel of sparflaxacin for sustained ocular drug delivery: in vitro and ex vivo characterization. *Pharm. Dev. Technol.* 20, 662–669. <https://doi.org/10.3109/10837450.2014.910807>.
- Khiev, D., Mohamed, Z.A., Vichare, R., Paulson, R., Bhatia, S., Mohapatra, S., Lobo, G.P., Valapala, M., Kerur, N., Passaglia, C.L., 2021. Emerging nano-formulations and nanomedicines applications for ocular drug delivery. *Nanomaterials* 11, 173. <https://doi.org/10.3390/nano11010173>.
- Koppa Raghu, P., Bansal, K.K., Thakor, P., Bhavana, V., Madan, J., Rosenholm, J.M., Mehra, N.K., 2020. Evolution of nanotechnology in delivering drugs to eyes, skin and wounds via topical route. *Pharmaceutics* 13, 167. <https://doi.org/10.3390/ph13080167>.
- Lee, C.H., Moturi, V., Lee, Y., 2009. Thixotropic property in pharmaceutical formulations. *J. Control. Release* 136, 88–98. <https://doi.org/10.1016/j.jconrel.2009.02.013>.
- Liu, Z., Zhang, X., Li, J., Liu, R., Shu, L., Jin, J., 2009. Effects of labrasol on the corneal drug delivery of baicalin. *Drug Deliv.* 16, 399–404. <https://doi.org/10.1080/10717540903126165>.
- Lu, D.-W., Tai, M.-C., Chang, Y.-H., Liang, C.-M., Chen, C.-L., Chien, K.-H., Chen, J.-T., Chen, Y.-H., 2013. Anterior chamber paracentesis and pH values in patients with acute primary angle closure. *Graefes Arch. Clin. Exp. Ophthalmol.* 251, 1229–1234. <https://doi.org/10.1007/s00417-012-2198-y>.
- Manca, M.L., Manconi, M., Nacher, A., Carbone, C., Valenti, D., Maccioni, A.M., Sinico, C., Fadda, A.M., 2014. Development of novel diolein-niosomes for cutaneous delivery of tretinoin: influence of formulation and in vitro assessment. *Int. J. Pharm.* 477, 176–186. <https://doi.org/10.1016/j.ijpharm.2014.10.031>.
- Mazed, E.A., Zakaria, S., 2019. Enhancement of dissolution characteristics of clodogrel bisulphate by proniosomes. *Int. J. App. Pharm.* 77–85. <https://doi.org/10.22159/ijap.2019v11i2.30575>.
- Mazed, E.A., Helal, D.A., Elkhouday, M.M., Abd Elhameed, A.G., Yasser, M., 2021. Formulation and optimization of nanospanlastics for improving the bioavailability of green tea epigallocatechin gallate. *Pharmaceutics* 14, 68. <https://doi.org/10.3390/ph14010068>.
- Miastkowska, M., Kulawik-Pióro, A., Szczurek, M., 2020. Nanoemulsion gel formulation optimization for burn wounds: analysis of rheological and sensory properties. *Processes* 8, 1416. <https://doi.org/10.3390/ph8111416>.
- Mohammed, M.H.H., Hamed, A.N.E., Elhabal, S.F., Mokhtar, F.A., Abdelmohsen, U.R., Fouad, M.A., et al., 2023. Chemical composition and anti-proliferative activities of Hypophorbe lagenicaulis aerial parts and their biogenic nanoparticles supported by network pharmacology study. *S. Afr. J. Bot.* 156, 398–410. <https://doi.org/10.1016/J.SAJB.2023.03.018>.
- Mohammed, M.H.H., Hamed, A.N.E., Elhabal, S.F., Mokhtar, F.A., Abdelmohsen, U.R., Fouad, M.A., et al., 2023a. Metabolic profiling and cytotoxic activities of ethanol extract of *Dypsis leptocheilos* aerial parts and its green synthesized silver nanoparticles supported by network pharmacology analysis. *S. Afr. J. Bot.* 161, 648–665. <https://doi.org/10.1016/J.SAJB.2023.08.026>.
- Olgac, S., Usta, D.Y., Inceciayir, T., 2021. Comparison of tablet splitting techniques for dosing accuracy of nebivolol tablets: hand splitting versus tablet cutter and knife. *Saudi Pharm. J.* 29, 1486–1491. <https://doi.org/10.1016/j.jsps.2021.11.005>.
- Onugwu, A.L., Nwagwu, C.S., Onugwu, O.S., Echezona, A.C., Agbo, C.P., Ihim, S.A., Emeb, P., Nnamani, P.O., Attama, A.A., Khutoryansky, V.V., 2023. Nanotechnology based drug delivery systems for the treatment of anterior segment eye diseases. *J. Control. Release* 354, 465–488. <https://doi.org/10.1016/j.jconrel.2023.01.018>.
- Pandey, M., Choudhury, H., Binti Abd Aziz, A., Bhattamisra, S.K., Gorain, B., Su, J.S.T., Tan, C.L., Chin, W.Y., Yip, K.Y., 2021. Potential of stimuli-responsive in situ gel system for sustained ocular drug delivery: recent progress and contemporary research. *Polymers* 13, 1340. <https://doi.org/10.3390/polym13081340>.
- Paul, D., 2011. Elaborations on the Higuchi model for drug delivery. *Int. J. Pharm.* 418, 13–17. <https://doi.org/10.1016/j.ijpharm.2010.10.037>.
- Qamar, Z., Qizilbash, F.F., Iqbal, M.K., Ali, A., Narang, J.K., Ali, J., Baboota, S., 2019. Nano-based drug delivery system: recent strategies for the treatment of ocular disease and future perspective. *Recent Pat. Drug Deliv. Formul.* 13, 246–254. <https://doi.org/10.2174/187221131466619122415211>.
- Qi, X., Xiang, Y., Cai, E., You, S., Gao, T., Lan, Y., Deng, H., Li, Z., Hu, R., Shen, J., 2022. All-in-one: harnessing multifunctional injectable natural hydrogels for ordered therapy of bacteria-infected diabetic wounds. *Chem. Eng. J.* 439, 135691. <https://doi.org/10.1016/j.cej.2022.135691>.
- Rathod, S., Arya, S., Shukla, R., Ray, D., Aswal, V.K., Bahadur, P., Tiwari, S.J.C., Physicochemical, S.A., Aspects, E., 2021. Investigations on the role of edge activator upon structural transitions in Span vesicles. *Colloids Surf. A Physicochem. Eng. Asp.* 627, 127246. <https://doi.org/10.1016/j.colsurfa.2021.127246>.
- Salem, H.F., Nafady, M.M., Kharshoum, R.M., Abd El-Ghafar, O.A., Farouk, H.O., 2020. Novel enhanced therapeutic efficacy of dapoxetine HCl by nano-vesicle transdermal gel for treatment of carrageenan-induced rat paw edema. *AAPS PharmSciTech* 21, 1–13. <https://doi.org/10.1208/s12249-020-01656-6>.
- Sammar Fathy Elhabal, M.A.E.-N., Abdelaal, Nashwa, Elrefai, Mohamed Fathi Mohamed, Ghaffar, Shrouk A., Khalifa, Mohamed Mansour, Mohie, Passant M., Waggas, Dania S., Hamdan, Ahmed Mohsen Elsaid, Alshawwa, Samar Zuhair, Saied, Essa M., Elzohairy, Nahla A., Elnawawy, Tayseer, Gadr, Rania A., Elfar, Nehal, Mohammed, Hanaa, Khasawneh, Mohammad Ahmad, 2023b. Development of canagliflozin nanocrystals sublingual tablets in the presence of sodium caprate permeability enhancer: formulation optimization, characterization, in-vitro, in silico, and in-vivo study. *Drug Deliv.* 30, 2241665. <https://doi.org/10.1080/10717544.2023.2241665>.
- Shamma, R.N., Sayed, S., Sabry, N.A., El-Samanoudy, S.I., 2019. Enhanced skin targeting of retinoic acid spanlastics: in vitro characterization and clinical evaluation in acne patients. *J. Liposome Res.* 29, 283–290. <https://doi.org/10.1080/08982104.2018.1552706>.
- Sharma, A., Pahwa, S., Bhati, S., Kudeshia, P., 2020. Spanlastics: a modern approach for nanovesicular drug delivery system. *Int. J. Pharm. Sci. Res.* 11, 1057–1065. [https://doi.org/10.13040/IJPSR.0975-8232.11\(3\).1057-65](https://doi.org/10.13040/IJPSR.0975-8232.11(3).1057-65).
- Shivakumar, H., Desai, B., Subhash, P., Ashok, P., Hulakoti, B., 2007. Design of ocular inserts of brimonidine tartrate by response surface methodology. *J. Drug Deliv. Sci. Technol.* 17, 421–430. [https://doi.org/10.1016/S1773-2247\(07\)50083-3](https://doi.org/10.1016/S1773-2247(07)50083-3).
- Shokry, M., Hathout, R.M., Mansour, S., 2018. Exploring gelatin nanoparticles as novel nanocarriers for Timolol Maleate: augmented in-vivo efficacy and safe histological profile. *Int. J. Pharm.* 545, 229–239. <https://doi.org/10.1016/j.ijpharm.2018.04.059>.
- Shoman, N.A., Saady, M., Teaima, M., Abdelmonem, R., El-Nabarawi, M.A., Elhabal, S.F., 2023. Merging konjac glucomannan with other copolymeric hydrogels as a cutting-

- edge liquid raft system for dual delivery of etoricoxib and famotidine. *Drug Deliv.* 30. <https://doi.org/10.1080/10717544.2023.2189630>.
- Song, K.C., Lee, H.S., Choung, I.Y., Cho, K.I., Ahn, Y., Choi, E.J., 2006. The effect of type of organic phase solvents on the particle size of poly (d, l-lactide-co-glycolide) nanoparticles. *Colloids Surf. A Physicochem. Eng. Asp.* 276, 162–167. <https://doi.org/10.1016/j.colsurfa.2005.10.064>.
- Srivastava, V., Chary, P.S., Rajana, N., Pardhi, E.R., Singh, V., Khatri, D., Singh, S.B., Mehra, N.K., 2023. Complex ophthalmic formulation technologies: advancement and future perspectives. *J. Drug Deliv. Sci. Technol.* 104317. <https://doi.org/10.1016/j.jddst.2023.104317>.
- Suhail, M., Fang, C.-W., Minhas, M.U., Wu, P.-C., 2021. Preparation, characterization, swelling potential, and in-vitro evaluation of sodium poly (styrene sulfonate)-based hydrogels for controlled delivery of ketorolac tromethamine. *Pharmaceutics* 14, 350. <https://doi.org/10.3390/ph14040350>.
- Tayel, S.A., El-Nabarawi, M.A., Tadros, M.I., Abd-Elsalam, W.H., 2013. Promising insensitizing in situ ocular nanoemulsion gels of terbinafine hydrochloride: design, in vitro characterization and in vivo estimation of the ocular irritation and drug pharmacokinetics in the aqueous humor of rabbits. *Int. J. Pharm.* 443, 293–305. <https://doi.org/10.1016/j.ijpharm.2012.12.049>.
- Tayel, S.A., El-Nabarawi, M.A., Tadros, M.I., Abd-Elsalam, W.H., 2015. Duodenum-triggered delivery of pravastatin sodium via enteric surface-coated nanovesicular spanlastic dispersions: development, characterization and pharmacokinetic assessments. *Int. J. Pharm. Sci. Res.* 483, 77–88. <https://doi.org/10.1016/j.ijpharm.2015.02.012>.
- Teaima, M.H., Mohamed, M.A.A., Abd El Rehem, R.T., Tayel, S.A., El-Nabarawi, M.A., Fouad, S.A., 2021. Enhanced transdermal delivery of bisoprolol hemifumarate via combined effect of iontophoresis and chemical enhancers: ex vivo permeation/in vivo pharmacokinetic studies. *Pharmaceutics* 13, 682. <https://doi.org/10.3390/pharmaceutics13050682>.
- Trivedi, H.R., Siriah, T.M., Puranik, P.K., 2020. Experimental design approach for development of novel microemulsion system and immediate release self microemulsifying tablet of nebivolol HCl. *Braz. J. Pharm. Sci.* 56 <https://doi.org/10.1590/s2175-97902019000418070>.
- Turan-Vural, E., Torun-Acar, B., Acar, S., 2012. Effect of ketorolac add-on treatment on intra-ocular pressure in glaucoma patients receiving prostaglandin analogues. *Ophthalmologica* 227, 205–209. <https://doi.org/10.1159/000333822>.
- van den Bergh, B.A., Wertz, P.W., Junginger, H.E., Bouwstra, J.A., 2001. Elasticity of vesicles assessed by electron spin resonance, electron microscopy and extrusion measurements. *Int. J. Pharm.* 217, 13–24. [https://doi.org/10.1016/s0378-5173\(01\)00576-2](https://doi.org/10.1016/s0378-5173(01)00576-2).
- Van Haute, D., Jiang, W., Mudalige, T., 2019. Evaluation of size-based distribution of drug and excipient in amphotericin B liposomal formulation. *Int. J. Pharm.* 569, 118603 <https://doi.org/10.1016/j.ijpharm.2019.118603>.
- Vijayanand, P., Patil, J., Reddy, M.V., 2016. Formulation, characterization and in vivo evaluation of novel edible dosage form containing nebivolol HCl. *Braz. J. Pharm. Sci.* 52, 179–190. <https://doi.org/10.1590/S1984-82502016000100020>.
- Zafar, A., Ahmad, J., Akhter, S., Addo, R.T., 2016. Nanotechnology for transcorneal drug targeting in glaucoma: challenges and progress. *J. Ocul. Drug Deliv.: Adv. Chall. Appl.* 75–99.
- Zafar, A., Alsaidan, O.A., Imam, S.S., Yasir, M., Alharbi, K.S., Khalid, M., 2022. Formulation and evaluation of moxifloxacin loaded bilosomes in-situ gel: optimization to antibacterial evaluation. *Gels* 8, 418. <https://doi.org/10.3390/gels8070418>.
- Zaki, R.M., Alfadhel, M.M., Alshahrani, S.M., Alsaqr, A., Al-Kharashi, L.A., Anwer, M.K., 2022a. Formulation of chitosan-coated brigatinib nanospanlastics: optimization, characterization, stability assessment and in-vitro cytotoxicity activity against H-1975 cell lines. *Pharmaceutics* 15, 348. <https://doi.org/10.3390/ph15030348>.
- Zaki, R.M., Ibrahim, M.A., Alshora, D.H., El Ela, A.E.S.A., 2022b. Formulation and evaluation of transdermal gel containing tacrolimus-loaded spanlastics: in vitro, ex vivo and in vivo studies. *Polymers* 14, 1528. <https://doi.org/10.3390/polym14081528>.